Universidade de Aveiro Departamento de Engenharia Cerâmica e do Vidro
2008 Departamento de Física

TATIANA MARIA PEREIRA CORREIA

LATTICE DYNAMICS AND RELAXATION MECHANISMS IN DOPED $SRTIO_3$ CERAMICS
DINÂMICA DA REDE E MECANISMOS DE RELAXAÇÃO EM CERÂMICAS DE $SRTIO_3$ DOPADAS

Universidade de Aveiro
2008
Departamento de Engenharia Cerâmica e do Vidro
Departamento de Física

TATIANA MARIA PEREIRA CORREIA

LATTICE DYNAMICS AND RELAXATION MECHANISMS IN DOPED $SRTIO_3$ CERAMICS
DINÂMICA DA REDE E MECANISMOS DE RELAXAÇÃO EM CERÂMICAS DE $SRTIO_3$ DOPADAS

dissertação apresentada à Universidade de Aveiro para cumprimento dos requisitos necessários à obtenção do grau de Mestre em Ciência e Engenharia de Materiais, realizada sob a orientação científica do Dr. Paula Maria Lousada Silveirinha Vilarinho, Professor Associado do Departamento de Engenharia Cerâmica do Vidro da Universidade de Aveiro e do Dr. Abílio de Jesus Monteiro Almeida, Professor Associado com agregação da Faculdade de Ciências da Universidade do Porto

o júri

presidente

Prof. Dr. Jorge Ribeiro Frade
professor catedrático da Universidade de Aveiro

Prof. Dr. Abílio de Jesus Monteiro Almeida
professor associado com agregação da Faculdade de Ciências da Universidade do Porto (co-orientador)

Prof. Dr. Paula Maria Lousada Silveirinha Vilarinho
professor associado da Universidade do Aveiro (orientador)

Prof. Dr. Joaquim Agostinho Gomes Moreira
professor auxiliar da Faculdade de Ciências da Universidade do Porto

acknowledgments

I sincerely would like to express my gratitude to my co-supervisor, Prof. Dr. Abílio Almeida, for his competent guidance, teaching and tremendous support. I would also like to thank my supervisor, Prof. Dr. Paula Vilarinho for all the supervisory guidance throughout this project. I wish to thank Prof. Dr. Renata Chaves for the inspiring discussions and help.
Thanks to Dr. Alex Tckach who provided good quality ceramics to the project as well as interesting discussions.
Thanks to Prof. Dr. Agostinho Moreira for sharing his professionalism which contributed greatly to my work. Thanks to Eng. Albano Costa for his patient in helping me at set-up process in the laboratory. I would also like to acknowledge Prof. Dr. Petzelt, whose expertise was indispensable for completion of this thesis.
Thanks to my mother, who helped me revising the written English for this thesis. Finally, many thanks to my friends and family for all their enormous support.

palavras-chave

Titanato de Estrôncio, cerâmicas, paraeléctrico quântico, TSDC, espectroscopia Raman.

resumo

Cerâmicas ferroeléctricas do tipo relaxador têm despertado um renovado interesse científico, devido às suas muitas aplicações em tecnologia: memórias dinâmicas de acesso aleatório, condensadores “bypass”, dispositivos com aplicações na gama das microondas, sensores piroeléctricos de baixa temperatura, etc. Estas aplicações estão associadas a problemas conceptuais, relacionados com a distribuição de agregados polares e suas interacções, e também com o efeito mediador das matrizes em que os agregados estão inseridos.

Este trabalho tem como objectivo principal o estudo das propriedades polares de cerâmicas em matrizes altamente polarizáveis. Entre os materiais fortemente polarizáveis, os paraeléctricos quânticos são os que mais se destacam. São muito sensíveis a defeitos, impurezas, tensões e campos eléctricos. Um dos mais interessantes é o paraeléctrico quântico Titanato de Estrôncio ($SrTiO_3$), que apresenta uma transição de fase para-antiferrodistorsiva a ~ 110 K e que para concentrações adequadas de dopantes podem ser induzidos estados ferroeléctricos ou do tipo relaxador, geralmente localizados a baixas temperaturas. Estes estados podem corresponder à activação de novas bandas Raman de primeira ordem, a valores elevados de constante dieléctrica e a diferentes processos de relaxação polares.

Assim, este trabalho está focado no estudo comparativo da rede, das propriedades dieléctricas e de relaxação polar em cerâmicas de $SrTiO_3$ dopadas com Ítrio, Lantânio e Manganês, designados pelos sistemas $Sr_{1-1.5x}La_xTiO_3$ (x=0.0133, 0.0533 and 0.13), $Sr_{1-1.5x}Y_xTiO_3$ (x=0.005 and 0.01), $Sr_{1-x}Mn_xTiO_3$ (x=0.01, 0.02 and 0.05) and $SrTi_{1-x}Mn_yO3$ (y=0.01 and 0.05). Estes sistemas foram sintetizados pelo método convencional. A sua microestrutura e a estrutura cristalográfica foram analisadas através de difracção de raios X, microscopia electrónica de varrimento e transmissão, assim como por espectroscopia de energia dispersiva. Estudos detalhados de dinâmica de rede e de processos polares foram realizados utilizando as técnicas de espectroscopia Raman e de Correntes Termicamente Estimuladas (CTE), num amplo intervalo de temperaturas variando entre 10 K e a temperatura ambiente. Os resultados experimentais foram analisados através de modelos teóricos e discutidos com base na estequiometria química, características dos iões e a sua localização na rede.

Pretende-se, a partir do conjunto de resultados obtidos, compreender melhor as propriedades do Titanato de Estrôncio. Embora, a dinâmica da rede do $Sr_{1-1.5x}La_xTiO_3$ (x=0.0133, 0.0533 and 0.0833) ter sido já estudada, o efeito da dopagem de Ítrio é ainda desconhecido.
No presente estudo, propomos analisar o espectro Raman obtido em ambos os sistemas e diferentes concentrações, com o objectivo de clarificar o comportamento da rede do $SrTiO_3$ aquando a dopagem por iões aliovalentes. Os resultados experimentais indicam que a substituição do ião de Estrôncio por iões de Lantânio e Ítrio, dá origem a novas bandas nos espectros Raman, devido à perda do centro de inversão originado pelo efeito de dopagem do Titanato de Estrôncio. Este facto permite o acesso ao comportamento das bandas activas em infravermelho, sendo assim possível obter informações relativas à existência de estados polares a baixas temperaturas. O amortecimento parcial do modo polar TO1 obtido em todos os sistemas estudados aponta para a ausência de uma fase ferroelétrica a baixas temperaturas, confirmando resultados publicados anteriormente.
O desvio da temperatura de transição para-antiferrodistorsiva para temperaturas mais elevadas nos sistemas dopados com Ítrio e Lantânio mostra que T_a é fortemente dependente do factor de tolerância da estrutura.
Apesar das mudanças observadas em T_a nos sistemas dopado de $SrTiO_3$, o comportamento em temperatura do modo mole associado à transição de fase antiferrodistorsiva A_{1g}, pode ser descrito em termos de uma lei de potência semelhante à lei utilizada em trabalhos previamente realizados no sistema de $SrTiO_3$ não dopado. Observam-se ainda alguns modos de baixa frequência, que por não poderem ser identificados com nenhum modo da rede, podem efectivamente estar associados a efeitos de desordem originados pela presença dos iões dopantes nestes sistemas.
Vários trabalhos focaram-se já no estudo do $SrTiO_3$ dopado, contudo os processos de relaxação polar observados em alguns destes sistemas não foram ainda completamente analisados. Assim, os processos de relaxação polar observados nas cerâmicas de $SrTiO_3$ dopadas com Lantânio,Ítrio e Manganês foram estudados a partir de medidas de Currentes Termicamente Estimuladas (CTE) na gama de temperatura 10-300 K. Os resultados experimentais obtidos foram analisados através de modelos de relaxação dipolar e cargas espaciais, com o objectivo de determinar a natureza dos processos de relaxação. Estes resultados revelam a existência de diferentes processos de relaxação localizados na gama de temperaturas estudada. Com base em resultados previamente publicados, os mecanismos de relaxação detectados por CTE nos sistemas estudados e que ocorrem a baixas temperaturas foram associados a mecanismos de origem dipolar, enquanto que aqueles que se observam a altas temperaturas foram atribuídos à deslocação de cargas espaciais.
Os resultados obtidos nos sistemas em que o ião dopante substitui o catião no lugar A ou B da rede apontam para a existência de mecanismos de relaxação polares muito distintos.
Considerando apenas os processos de tipo dipolar observados a baixas temperaturas, foi possível identificar os correspondentes mecanismos de relaxação e concluir que estes dependem principalmente do raio iónico do ião dopante e do nodo da rede onde a substituição ocorre. Esta técnica (CTE) não convencional tem revelado ser de grande interesse como complemento de resultados previamente obtidos por espectroscopia dieléctrica.
Esta dissertação é constituída por quatro principais capítulos. O capítulo 1 inclui uma revisão da literatura sobre materiais relacionados com SrTiO3 e concluí com os objectivos deste trabalho. No capítulo 2 são apresentados resultados referentes à dinâmica da rede dos sistemas $Sr_{1-1.5x}La_xTiO_3$ e $Sr_{1-1.5x}Y_xTiO_3$ obtidos por espectroscopia Raman. Ainda neste capítulo, é introduzido o fenómeno da difusão Raman e apresentada um estudo comparativo da transição de fase para-antiferodistorsiva e a natureza paraléctrica quântica destes dois sistemas.

Uma técnica distinta foi também utilizada na identificação dos mecanismos de relaxação em cerâmicas de $SrTiO_3$ dopadas: Correntes Termicamente Estimuladas (CTE). No capítulo 3, este método eficaz é descrito e aplicado no estudo das cerâmicas de $SrTiO_3$ dopadas com Lantânio, Ítrio e Manganês. Neste capítulo é desenvolvida uma discussão geral que relaciona estes resultados com os resultados apresentados na literatura. A análise teórica dos resultados experimentais permitirá uma melhor compreensão dos processos de relaxação observados a partir da determinação dos parâmetros característicos, tais como a energia de activação e tempo de relaxação a temperatura infinita. Esta informação proporcionará a identificação dos mecanismos subjacentes ao comportamento de relaxador anteriormente observado. Finalmente, os resultados obtidos serão resumidos no capítulo 4, bem como apresentadas algumas sugestões de trabalho futuro.

keywords

Strontium Titanate, ceramics, quantum paraelectric, TSDC, Raman spectroscopy.

abstract

Ferroelectric ceramics and relaxors have awaken a renewed scientific interest, due to their many applications in technology: dynamic random access memories (DRAMs), bypass capacitors, tuneable microwave devices, low temperature pyroelectric sensors, etc. These applications are associated with conceptual problems, which deal with the distribution of polar aggregates and their interactions, and also with the mediator effects of the matrices in which the aggregates are inserted.

This work is centred in the study of the properties of polar ceramics in highly polarizable matrices. Among the highly polarizable materials the quantum paraelectrics stand out. Their electrical properties are very sensitive to defects, impurities, stresses, and applied electric fields. One of the most interesting quantum paraelectrics is Strontium Titanate ($SrTiO_3$), which presents a para-antiferrodistortive phase transition at ~110 K and atomic lattice substitutions can induce ferroelectric or relaxor states, commonly located at low temperatures. These may yield the activation of Raman first order bands, high dielectric constant values and distinct polar relaxation processes.

Consequently this work is focused on the comparative study of the lattice, dielectric and polar relaxation properties of $SrTiO_3$ ceramics doped with Yttrium, Lanthanum, and Manganese ions, namely $Sr_{1-1.5x}La_xTiO_3$ (x=0.0133, 0.0533 and 0.13), $Sr_{1-1.5x}Y_xTiO_3$ (x=0.005 and 0.01), $Sr_{1-x}Mn_xTiO_3$ (x=0.01, 0.02 and 0.05) and $SrTi_{1-x}Mn_yO3$ (y=0.01 and 0.05) systems.

These systems were synthesised by the conventional mixed oxide method. Their crystallographic and micro structures were analysed through X-ray diffraction, scanning and transmission electron microscopy, together with energy dispersive spectroscopy methods. Detailed studies of both lattice dynamics and polar relaxations processes have been carried out through Raman and Thermally Stimulated Currents techniques, in a wide interval of temperatures ranging between 10 K and room temperature. The experimental results have been analysed through comprehensive theoretical models, and discussed on the basis of charge and chemical stoichiometry, ion characteristics, and site occupancy.

With the ensemble of these results it is expected to provide a better understanding of the physical properties of Strontium Titanate. Although, lattice dynamics of $Sr_{1-1.5x}La_xTiO_3$ (x=0.0133, 0.0533 and 0.0833) have already been reported, the Yttrium doping effect is still unknown.

In the present work we propose to analyze Raman spectra for both systems and different concentrations in order to clarify the aliovalent doping behaviour on $SrTiO_3$ lattice.

The obtained results show that Lanthanum and Yttrium substitution gives rise to new features in the Raman spectra, due to the loss of the center of inversion originated by doping $SrTiO_3$ ceramics. Those features enable us to have also access to the behavior of infrared active bands, which provides additional information regarding the existence of polar states at low temperatures. The absence of the softening of the TO_1 polar mode in all the systems studied supports the non-existence of a ferroelectric phase at low temperatures, which has been reported previously. The shift of the para-antiferrodistortive transition temperature (T_a) towards higher temperatures on both Lanthanum, and Yttrium doped systems clearly evidences that T_a is strongly dependent on the structural tolerance factor. Despite the observed changes in T_a in doped $SrTiO_3$, the temperature behaviour of the antiferrodistortive soft mode A_{1g} can be described in terms of a power law as it has been previously reported for pure $SrTiO_3$. Moreover some low frequency modes, which could not be assigned to other lattice modes, may be apparently associated with disorder effects, stemming from the presence of dopants ions.

Although there are several works addressed to the study of doped $SrTiO_3$ systems, the polar relaxation processes observed in some of these systems have not been fully investigated. Therefore, polar relaxation processes in La-, Y- and Mn- doped $SrTiO_3$ ceramics were studied by undertaking Thermally Stimulated Currents (TSC) measurements from room temperature to 10 K. The experimental results were analyzed by using dipolar and space-charge relaxation models in order to determine the nature of the relaxation processes involved. The results reveal the existence of different relaxation processes within the studied range of temperatures. Whereas at low temperatures (18-80 K), relaxation mechanisms of dipolar type were disclosed, space-charge relaxation processes could be identified at higher temperatures (150-300 K) confirming the previous dielectric results. In addition differences in the relaxation processes are observed for different substitute site of the lattice. Regarding dipolar relaxation processes observed at low temperatures, we were able to identify the corresponding mechanisms, which mainly depend on the ionic size, charge and site occupancy. This non conventional technique (TSC technique) has revealed to be a powerful technique to complement the results previously obtained by dielectric spectroscopy.

This thesis will comprise four main chapters. Chapter one includes a survey of literature addressing the background of $SrTiO_3$-related materials and concludes with the aims and objectives of this work. Chapter 2 disclose the lattice dynamics of $Sr_{1-1.5x}La_xTiO_3$ and $Sr_{1-1.5x}Y_xTiO_3$ systems revealed by Raman spectroscopy. Here, Raman diffusion theory is briefly introduced as well as the experimental set-up used in this work. This chapter concludes with a comparison between both systems regarding the para-antiferrodistortive phase transition and quantum paraelectricity features. A different technique was used to identify relaxation mechanisms in doped $SrTiO_3$: Thermally Stimulated Depolarization Currents (TSDC) technique. In Chapter 3, this powerful method is reviewed and applied to La-, Y- and Mn- doped $SrTiO_3$ ceramics. This chapter outlines the general discussion and links the results to the literature survey from the Chapter 1. The theoretical analysis of the experimental data should enable us to gain a better understanding of the relaxation processes through the knowledge of their characteristic parameters such as the activation energy, and relaxation time at infinite temperature. This information will allow determining which mechanisms are underlying the relaxation behaviour previously reported. Finally, a summary of the results obtained for the studied systems is presented in Chapter 4, which ends with a few concluding remarks and directions for further work.

CONTENTS

TABLE OF FIGURES

TABLE OF TABLES

1 Introduction: Background and Literature survey

A brief introduction to the structure and properties of undoped Strontium Titanate ($SrTiO_3$) will be presented in this chapter. This is followed by a review of the known behaviour of doped $SrTiO_3$, in particular Y- and La- doped materials. Finally, a description of the motivation and the objectives for the work herein contained will be given.

1.1 Undoped $SrTiO_3$

1.1.1 Structure of $SrTiO_3$

Strontium Titanate oxide crystallizes with the perovskite type structure with the general formulae ABO_3. Generally, in a perovskite structure, B-site ions (transition metal ions) determine the basic properties of the materials, while A-site ions (rare earth ion or alkali-earth metal) establish the valence of B- site ions and the distortion of the lattice, depending on their radii. Hence, one of the methods most frequently employed to change the material properties and their ground state is the chemical substitution of A-site ions as carrier doping determines charges, spins, and anisotropic orbits of materials.

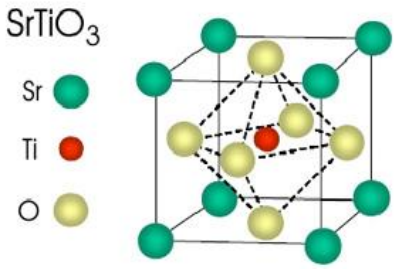

Figure 1-1 $SrTiO_3$ perovskite structure[1].

The cubic perovskite structure of $SrTiO_3$ is shown in Figure 1-1. At room temperature (space group P*m3m*), the cubic unit cell consists of a central Ti^{4+} ion (B-site), which is octahedrally coordinated by six O^{2-} ions. Moreover, Sr^{2+} ions (A-site) are located at the corners of the cubic unit cell. Figure 1-2 illustrates the $SrTiO_3$ structure visualized as a

three-dimensional framework. It can be seen that Ti^{4+} ions are at the centre of oxygen octahedra (TiO_6 octhaedral units), with Sr^{2+}-ions in the centre of the vacant space between them[1].

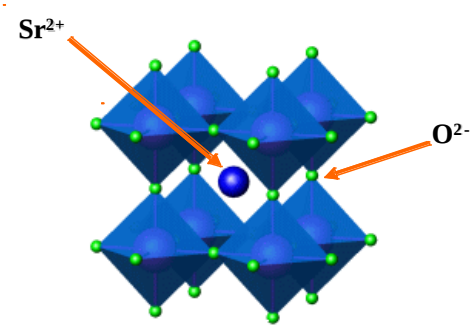

Figure 1-2 The cubic perovskite structure of $SrTiO_3$: TiO_6 octhaedral units[1].

1.1.2 Structural and ferroelectric instabilities

In general, perovskites exhibit two sorts of instabilities that may compete with each other: i) structural- linked to the rotations of BO_6 octahedra, and ii) ferroelectric- caused by polar displacements within B-O bonds. In the particular case of $SrTiO_3$, the antiferrodistortive transition, which occurs at T_C = 105 K, is associated with the rotation of the TiO_6 octahedra. However, Muller and Burkhard[2] reported that pure $SrTiO_3$ single crystals exhibit a dielectric constant that increases with decreasing temperature, though remaining constant below 4 K (Figure 1-3). Therefore, no phase transition into a ferroelectric state can be observed in $SrTiO_3$ at low temperatures.

From 300 K down to 70 K, the permittivity of $SrTiO_3$ follows the Curie-Weiss law. Nevertheless, a deviation from this law can be seen below 50 K[2] (Figure 1-3), which, according to Barret, is associated with quantum fluctuation effects[3]. For this reason, $SrTiO_3$ is usually known as an incipient ferroelectric or a quantum paralelectric. The origin of such quantum effects is likely to be associated with the uncertain position of the Ti^{4+} ion within the oxygen octahedral. Saturation of the ferroelectric TO1 mode reveals that these quantum fluctuations tends to suppress the ferroelectric order at low temperatures[2].

The phonon structure plays a crucial role in the outstanding quantum paraelectric behaviour of $SrTiO_3$.

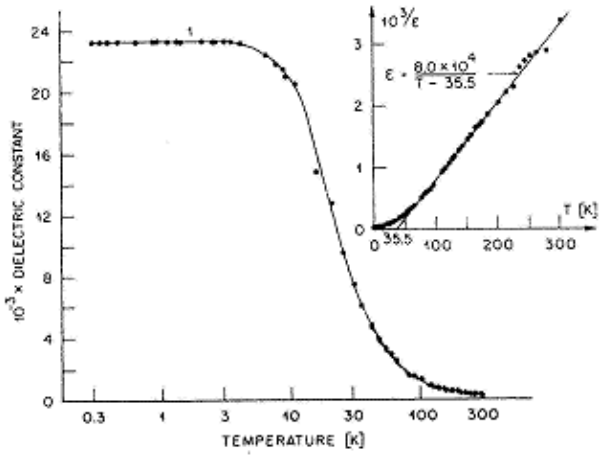

Figure 1-3 Dielectric constant of $SrTiO_3$ crystal as a function of temperature (adapted)[2].

As one can see in Figure 1-4, the antiferrodistortive modes (A_{1g}, non-degenerate, and E_g, doubly degenerate) soften to zero energy at the phase transition near 105 K. On the other hand, ferroelectric modes, non-degenerate A_{2u} branch and a doubly degenerate E_u branch, do not completely collapse to zero energy at finite temperatures, due to the effect of quantum fluctuations that become greater at low temperatures.

Moreover, a field-induced temperature dependence of dielectric permittivity reveals other interesting properties of Strontium Titanate (Figure 1-5). Low temperature dielectric permittivity decreases under d.c. fields (0 to 150 V/mm), exhibiting a broad peak in ε`(T) for E_{bias} > 200 V/mm. The observed maximum of the dielectric permittivity was associated with the onset of field induced polarisation at low temperatures[5].

According to Muller *et al.*[6], a spontaneous phase transition occurs at T~ 37 K, leading to a novel coherent quantum state. Arzel *et al.*[7] have suggested that these low-T anomalies of $SrTiO_3$ are "bulk" ones and that antiphase domain boundaries can undergo a ferroelectric transition at low temperatures. Conversely, elastic measurements in $SrTiO_3$ single crystals[8] indicated that effects found near 37 K are purely dynamic and not an indication of structural phase transition. Despite enormous effort, this feature is not yet thoroughly understood.

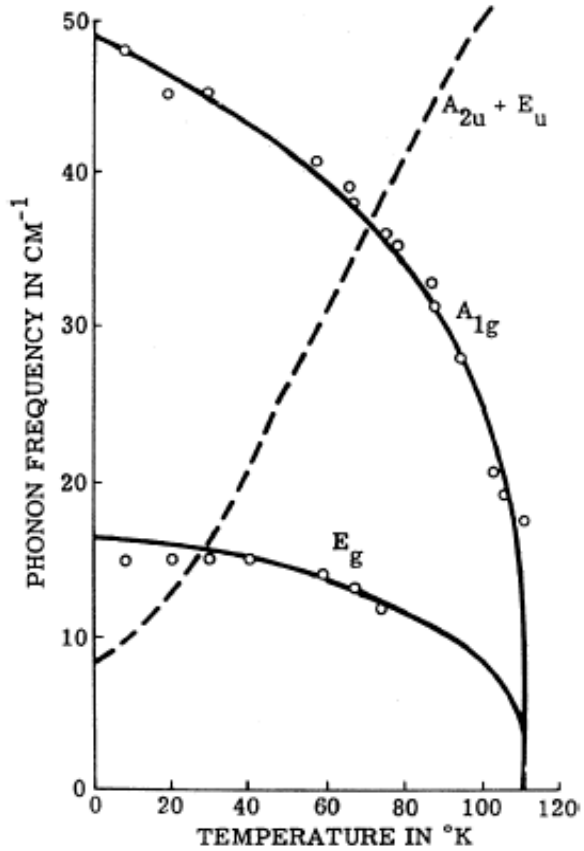

Figure 1-4 Soft optical frequencies versus temperature of $SrTiO_3$ single crystals[4].

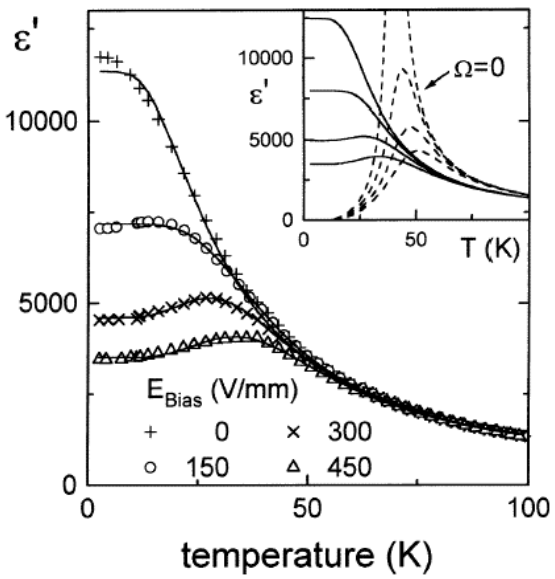

Figure 1-5 Dielectric constant of $SrTiO_3$ crystal as a function of temperature and electric field[5].

Lately, great attention has been paid to the study of $SrTiO_3$ ceramics[9], although the values of dielectric permittivity at low temperatures are several times smaller than in single crystals and, microwave losses higher and grain size dependent. Lower permittivity, which implies lesser, softening of the soft mode, was established to be mainly related to the existence of micro-polar regions in undoped $SrTiO_3$ ceramics, apparently due to frozen dipole moments at the grain boundaries[9].

Raman spectra were obtained for $SrTiO_3$ ceramics at different temperatures (Figure 1-6)[9]. Apart from second-order features that dominate the spectra at room temperature, Petzelt *et al.*[9] have observed that, as in single crystals, TO1 mode in ceramics does not reach zero frequency due quantum fluctuations (see Figure 1-7). Besides, the same author reported that the para-antiferrodistortive phase transition temperature shifts towards higher temperatures, from 105 K in single crystals to 132 K for ceramics.

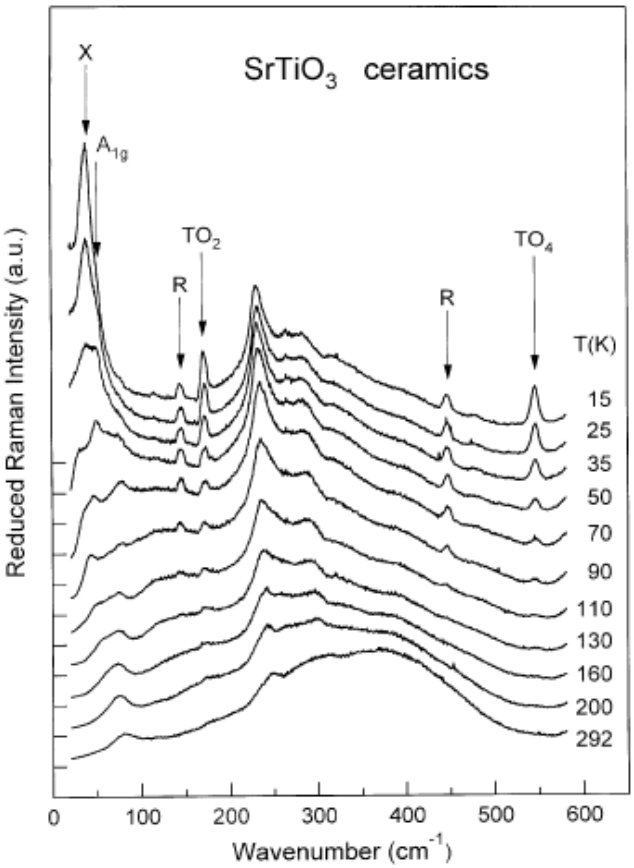

Figure 1-6 Raman spectra of $SrTiO_3$ ceramics at different temperatures[9].

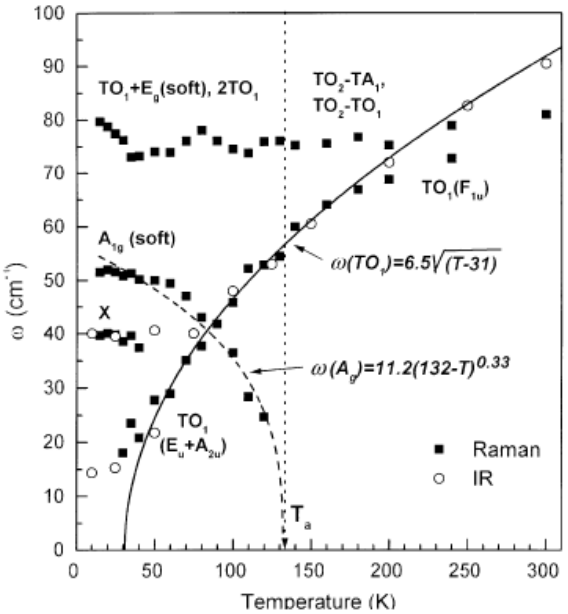

Figure 1-7 Temperature dependence of mode frequencies below 100 cm^{-1}[9].

Table 1-1 below sums up the phonon modes frequencies for pure $SrTiO_3$ ceramics. Herein, some modes are designated as (IR) and others as (R), signifying that these modes are only visible in Infrared and Raman spectra, respectively.

MODES	5 K	80 K	160 K	300 K
TO1 (A_{2u}+E_u)	18	40 (R)	63	94 (IR)
$R'^{E_g}_{A_g}$	41 (R)	-	-	-
R'_{25} (B_{1g}+E_g)	146 (R)	145 (R)	-	-
LO1 (A_{2u}+Eg)	169 (IR)	170 (IR)	170 (IR)	171 (IR)
TO2 (A_{2u}+E_u)	172	173	173	175 (IR)
R12 (B_{2g})	231 (R)	233 (R)	-	-
F_{2u} (TO3 + LO2)	264 (R)	265 (R)	-	-
R_{15} (E_u− TO +LO)	436 (IR)	439 (IR)	-	-

R`$_{25}$ (B_{1g} + E_g)	449 (R)	447 (R)	-	-
LO3 (A_{2u} + E_u)	474 (IR)	475 (IR)	475 (IR)	473 (IR)
TO4 (A_{2u} + E_u)	548	550 (R) 544 (IR	545 (IR)	545 (IR)
LO4 + R_1(A_{2g})	795	796	796	796

Table 1-1 Phonon mode frequencies (cm^{-1}) in $SrTiO_3$ ceramics[11].

1.2 Doped $SrTiO_3$

As reported previously, a polar state in $SrTiO_3$ solid solutions can be easily achieved by the application of a strong electric field or uniaxial stress, isotope substitution of O^{2-}, anion or Sr^{2+} iso- or heterovalent cation substitution.

The introduction of impurities in $SrTiO_3$ also induces profound changes in its physical properties. Doping of $SrTiO_3$ can be achieved by substitutions on the Sr^{2+} site (or A-site), and Ti^{4+} site (or B-site) with diverse dopants.

According to previous data[12], ferroelectricity can be induced when isovalent cations such as Ba^{2+}, Ca^{2+}, Cd^{2+}, Pb^{2+}, Mn^{2+} are added to $SrTiO_3$ lattice. However, in certain dopant concentration ranges, a relaxor state may be observed for some of these systems revealed by dielectric diffuse anomalies with wide frequency dispersion at radio frequencies and the temperature dependence of the shift of the maximum of the anomaly. The same relaxor behaviour was also obtained for nonisovalent cations, bismuth (Bi^{3+}) and rare-earth ions[11,13]. Recently, a number of papers have been published where it is stated that Manganese and Lanthanum substitution does not induce any ferroelectric state at low temperatures[11,14].

On the other hand, iso- and heterovalent substitution of B-site leads to a smaller effect on dielectric properties than the one resulting from A-site doping.

Ferroelectricity and dielectric relaxor behaviour in doped $SrTiO_3$ has been associated with both cooperative displacements of Ti^{4+} ions in loosely packed oxygen octahedra, and polar clusters formed by off-centre dopant ions with high electronic polarisability[15].

Table 1-2 summarizes the dielectric behaviour of several doped $SrTiO_3$ bulk materials and a tentative assignment of the nature of its underlying mechanisms. A question mark is used whenever it is not clear what kind of mechanism is associated with the corresponding dielectric behaviour.

DOPANT IONS	SAMPLE TYPE	SITE	DIELECTRIC BEHAVIOUR	POLAR MECHANISM	REF
Zr^{4+} Sn^{4+} Ge^{4+}	Crystals	B-site	Very small effect in the dielectric properties relatively to A-site.	?	[14]
Ba^{2+} Cd^{2+} Pb^{2+}	Ceramic/Crystal	A-site	Ferroelectric and relaxor-type behaviour.	Cooperative displacements of Ti^{4+} ions in loosely packed oxygen octahedral.	[14]
Ca^{2+}	Ceramic	A-site	Ferroelectric and relaxor-type behaviour.	Polar clusters formed by off-centre dopant ions.	[14]
Bi^{3+}	Ceramic	A-site	Ferroelectric and relaxor-type behaviour.	Polar clusters formed by off-centre dopant ions with high electronic polarisability.	[13,11]
La^{3+}	Ceramic	A-site	Relaxor-type behaviour.	Bulk and grain boundary dipoles and surface charge release	[11]

Y^{3+}		A-site	Relaxor-type behaviour	?	[16]
Mn^{2+}	Ceramic	A-site	Ferroelectric relaxoroff-centre shift of dopant ions in Sr^{2+} site	off-centre shift of dopant ions in Sr^{2+} site	[14,18]
Mn^{4+}	Ceramic	B-site	Incipient ferroelectric behaviour	Quantum fluctuations become more stable	[14,19]

Table 1-2 Dielectric behaviour of doped $SrTiO_3$.

As shown in Table 1-2, some uncertainties remain regarding doped $SrTiO_3$ ceramics. Bismuth, Lanthanum and Yttrium ions have similar charge and ionic radius, which leads to the same type of A-site doping. Due to this fact, Bi- and La-doped $SrTiO_3$ ceramics exhibit several and similar relaxation processes, though Bismuth incorporation shows also an anomaly in the dielectric response. On the other hand, only a few investigations have addressed to the study of Y-doped $SrTiO_3$ ceramics. Therefore, some work is still missing in order to determine the nature of the relaxation mechanisms underlying heterovalent $SrTiO_3$ doping.

In spite of the several works focused on Mn-doped $SrTiO_3$ system, the effect of Manganese A- and B-site doping on the polar and dynamic properties of $SrTiO_3$ is still under debate, due to the uncertainty regarding the dopant lattice site occupancy.

1.2.1 The effect of Lanthanum doping on $SrTiO_3$ properties

The incorporation of La^{3+} on A-site of the Strontium Titanate lattice, due to the charge imbalance was assumed to be compensated by the formation of Strontium vacancies, as $Sr_{1-1.5x}La_xTiO_3$[13].

The temperature dependence of ε` for La-doped $SrTiO_3$ at 10 kHz (Figure 1-8) reveals that, for x>0.10, peaks are observed at around 200-300 K, and for x<0.10, dielectric

permittivity increases monotonically with decreasing temperature[15]. Nevertheless, for all doping concentrations studied the maximum value of the dielectric permittivity decreases with the introduction of Lanthanum into the lattice.

La-doped $SrTiO_3$ is recognised as a non-ferroelectric system, as no hysteresis loops have ever been observed. Furthermore, two sets of permittivity peaks were found by Iguchi *et al.*[19] in the temperature range 25 K to 300 K in $Sr_{1-1.5x}La_xTiO_3$ ceramics with $0.006<x<0.03$. The physical nature of their dielectric behaviour was described by using the Skanavi model. Later, Yu[13] obtained a similar dielectric response in $Sr_{1-1.5x}La_xTiO_3$ and demonstrated that the observed permittivity peaks were not due the lattice but oxygen vacancies.

Recently, a study of pyroelectric thermal cycles and dielectric constant in La-doped $SrTiO_3$ ceramics[11] was carried out, revealing complex non-ergodic behaviour associated with the existence of different relaxation processes. Apparently, they are due to either bulk/grain boundary dipole reorientation or surface charge release. These results agree with previous works since no ferroelectric behaviour was observed in pyroelectric currents neither in dielectric constant.

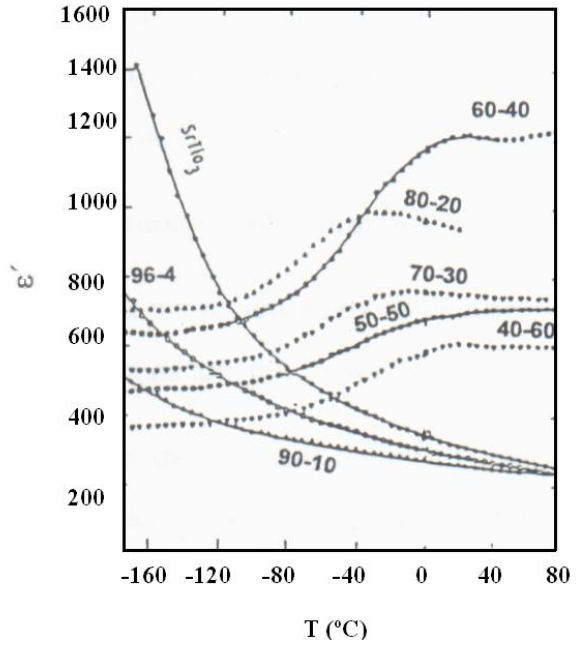

Figure 1-8 Temperature dependence of ε` for La-doped $SrTiO_3$ ceramics at 10 kHz[14].

The introduction of lanthanum leads to drastic changes of the lattice dynamics of the undoped $SrTiO_3$ system that have been associated with both internal stress and structural disorder[11]. This statement stems from both the huge increase of the para-antiferrodistortive phase transition temperature as the lanthanum content increases, and the absence of a polar state at low temperatures, thoroughly supported by Raman measurements[11] and in situ TEM measurements as well[21].

1.2.2 The effect of Yttrium doping on $SrTiO_3$ properties

Recently, much attention has been given to the study of the Yttrium-doped $SrTiO_3$ system as it has been considered as an anode material for solid oxide fuel cells[21].
Current studies have revealed that Y^{3+} ions substitute the Sr^{2+} site and may operate as donor substitution in the $SrTiO_3$ lattice, which can be compensated either by the reduction of Ti^{4+} to Ti^{3+} or originating Sr^{2+} vacancies[22]. Moreover, no paraelectric-quantum ferroelectric transition has been observed in Y-doped $SrTiO_3$[23]. Instead, dielectric properties have disclosed the existence of a ε' peak at low temperature, as shown in Figure 1-9.

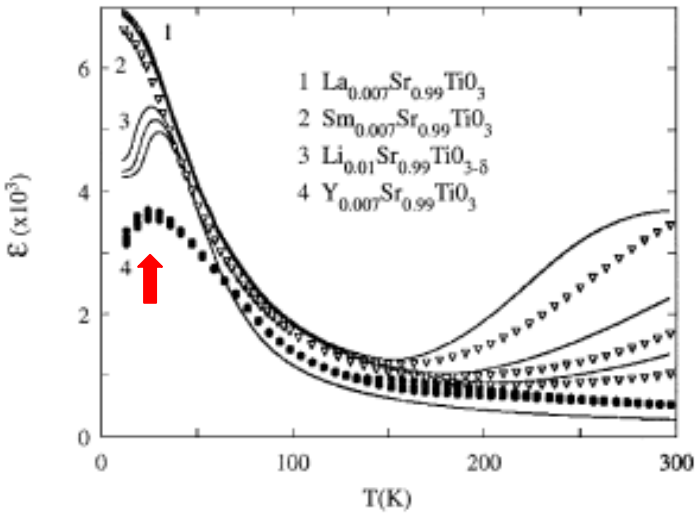

Figure 1-9 Temperature variation of dielectric constant for heterovalent substituted $SrTiO_3$ at 10, 100, and 500 kHz[23].

Albeit tentatively, some authors have suggested that this peak is associated with a dipole-glass transition, the origin of which is not yet clearly understood. In fact, a small number of works has addressed the study of this system, particularly its dynamic and dielectric properties[24].

Due to its extremely interesting physical properties, the Y-doped $SrTiO_3$ system appears to be very promising for emergent practical applications. Nonetheless, further study is required to take advantage of its physical properties more comprehensively and to improve the understanding of the different aliovalent dopants effect in $SrTiO_3$.

1.2.3 The effect of Manganese doping on $SrTiO_3$ properties

The first report concerning Mn-doped $SrTiO_3$ was published by Muller[25]. An EPR (Electron Paramagnetic Resonance) spectrum was obtained for single crystals, attributed to Mn^{4+} substitution of Ti^{4+}[25]. The proximity of ionic sizes between Mn^{4+} and Ti^{4+} supports this hypothesis. The author observed that thermal annealing in reducing atmosphere leads to the decrease of valence state ions converting Mn^{4+} into Mn^{3+} or Mn^{2+}, where the charge compensation mechanism is established by oxygen vacancies[25]. Due to a multivalent ionic state, Manganese ions were later associated with both Sr^{2+} and Ti^{4+} site substitution. Lemanov and co-workers[26] observed dielectric relaxation in $SrMn_yTi_{1-y}O_3$, suggesting that this behaviour derives from the reorientation of polarons located at $\{Mn^{2+}_{Ti} - O^{-}\}$-type defects. Recently, radio-frequency dielectric measurements[18] were carried out focusing on the effect of A- and B-site substitution on its dielectric properties[18]. For the case of B-site doping, the temperature dependence of the $SrTi_{1-y}Mn_yO_3$ dielectric constant shown in Figure 1-10 reveals that Mn^{4+} substitution of Ti^{4+} does not originate any anomaly but rather a mere decrease of the dielectric constant.

It seems acceptable that Mn^{4+} incorporation into a Ti^{4+} site leads to a decrease of the packing degree, which is favourable to the off-centre positioning of these ions and therefore, no ferroelectricity is detected since quantum fluctuations become more stable.

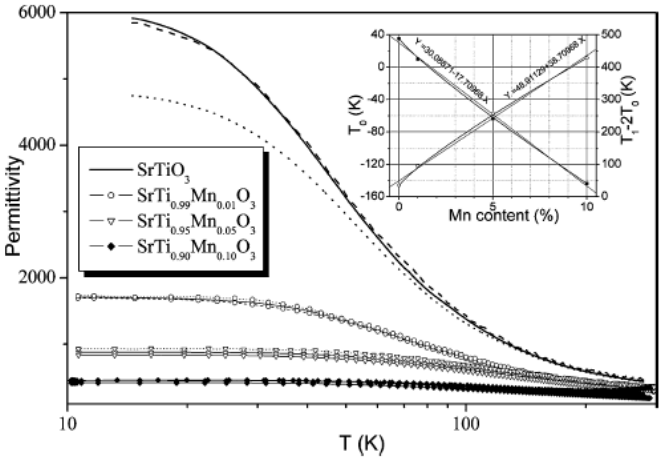

Figure 1-10 Temperature dependence of $SrTi_{1-y}Mn_yO_3$ dielectric permittivity at 10^2, 10^4 and 10^6 Hz; critical temperatures as a function of Mn content[18].

On the other hand, the $Sr_{1-x}Mn_xTiO_3$ system clearly shows a low-temperature dielectric relaxation[27] as observed by the systematic dielectric spectroscopy and dielectric relaxation analysis carried out in the $Sr_{1-x}Mn_xTiO_3$ system (see Figure 1-11).

The proposed relaxation mechanisms observed in Mn-doped $SrTiO_3$ is based on the off-centre hopping of Mn^{2+} at Sr^{2+} lattice sites. In addition, they observed that soft-mode phonon effect on the dielectric response decreases with the increasing of Mn^{2+} concentration, disappearing when the interaction between off-centred ions and polar clusters becomes more pronounced. Furthermore, a shift of soft mode to higher frequencies was also reported in the authors work[12].

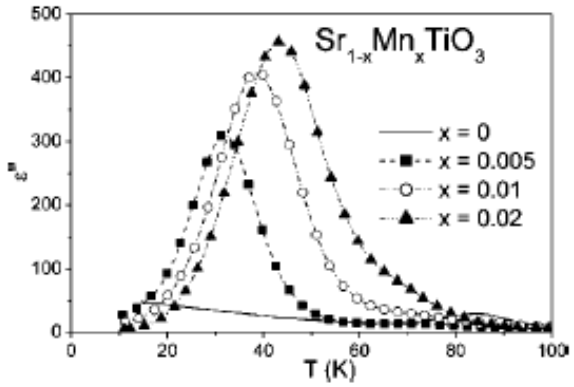

Figure 1-11 Temperature dependence of ε` of $Sr_{1-x}Mn_xTiO_3$[27].

1.3 Aim and Objectives

The lattice dynamic and electrical behaviour of some doped $SrTiO_3$ systems and the underlying mechanisms are still not completely understood, and still inspired much controversy. Researchers working on $SrTiO_3$ related materials have not been able to come to a consensus as to what physical processes are associated with the doping of $SrTiO_3$ perovskite structure. In addition, it is largely unknown in what measure the granular nature of ceramics influences the electrical and dynamic properties of some doped $SrTiO_3$ solid solutions.

It is well known that $SrTiO_3$ is characterized by a para-antiferrodistortive phase transition at 105 K, for single crystals, and 132 K, for ceramics. How its particular physical properties, and related parameters, such as the change in transition temperature are influenced by the introduction of some impurities is one of the purposes of this work. Particularly, the introduction of aliovalent ions with similar charge, like La^{3+} and Y^{3+}, was studied in the present work. Although, lanthanum doping (1%, 5% and 8% of lanthanum concentration) in $SrTiO_3$ lattice was reported to lead to an increasing of T_a, the behaviour of Yttrium incorporation is completely unknown. For this reason, A_{1g} mode behaviour was investigated in Y- and La- doped $SrTiO_3$ by Raman spectroscopy. Moreover, several previous investigations have pointed out that the introduction of some impurities, like barium and calcium, induce polar instabilities at low temperatures. Therefore, we will place particular emphasis on the TO_1 soft mode behaviour for Y- and La- doped systems.

During the last years, several authors attempt to describe the dielectric behaviour of doped $SrTiO_3$ systems. Particularly, it has been reported a relaxor behaviour for some dopants, such as bismuth and manganese. In this work, we aim to clarify and confirm the origin of such behaviour in La-, Y- and Mn- doped $SrTiO_3$ ceramics by thermal stimulated currents methodology. The underlying model will allow us to determine the nature of such relaxor mechanisms obtaining their characteristic parameters.

A detailed study of dynamic and relaxation properties concerning Mn-, La-, and Y-doped $SrTiO_3$ are herein complemented with a comparative analysis involving the results previously reported for other doped $SrTiO_3$ systems.

2 Raman Spectroscopy on $Sr_{1-1.5x}La_xTiO_3$ and $Sr_{1-1.5x}Y_xTiO_3$

Raman diffusion was discovered in 1928, almost at the same time, in India by Raman, and in Russia by Landsberg and Mandelston. When a transparent material is exposed to a monochromatic radiation with frequency υ_0, most of it is diffused either with no frequency change or inelastically. The former corresponds to Rayleigh scattering (υ_0), and the latter to Raman diffusion. The set of the new frequencies ($\upsilon_0 \pm \upsilon_R$) associated with photon absorption and emission characterizes the Raman spectrum.

Raman diffusion was predicted by quantum theory, though it is also explained within the scope of classical physics.

The great interest of Raman phenomena lies in their relation to the study of lattice dynamics in a large set of materials, such as crystalline materials, ceramics, thin films, etc. The close relation between Raman, symmetry and structural data often enables a better understanding of a large range of phenomena, wherever both structural and symmetry change occur.

2.1 Raman diffusion

2.1.1 Classic analysis of Raman scattering

When a system is exposed to radiation, characterized by an electric field $\vec{E} = \vec{E}\cos(\omega_0 t)$, an electric dipole moment $\vec{P}$ is induced in the material that can be described as:

$$\vec{P} = \vec{P}_1 + \vec{P}_2 + \vec{P}_3 + ...$$

In the description of the first order Raman effect, the linear term $\vec{P}_1$ is only considered and can be defined as

$$\vec{P}_1 = \vec{\vec{\alpha}}\vec{E}_0 \cos(\omega_0 t) \quad (2\text{-}1)$$

where $\vec{\vec{\alpha}}$ is the polarizability tensor.

The variations induced by the incident radiation in the vibration modes of the system can be represented in terms of the normal coordinates. Expanding this tensor in Taylor

series, considering only one normal coordinate Q_k, and neglecting all the terms that involve powers higher than the unity, the following expression is obtained

$$\vec{\vec{\alpha}}_k = \vec{\vec{\alpha}}_0 + \vec{\vec{\alpha}}_k' Q_{k0} \cos(\omega_k t + \delta_k) \quad (2\text{-}2)$$

where Q_{k0} represents the vibration normal coordinate of the associated nucleus at vibration frequency ω_k.

Combining both expressions 2-1 and 2-2, the polarization $\vec{P}_1$ is obtained:

$$\vec{P}_1 = \vec{\vec{\alpha}}_0 E_0 \cos(\omega_0 t) + \vec{\vec{\alpha}}_k' Q_{k0} \cos(\omega_k t + \delta_k) E_0 \cos(\omega_0 t) =$$
$$= \vec{\vec{\alpha}}_0 E_0 \cos(\omega_0 t) + \tfrac{1}{2} \vec{\vec{\alpha}}_k' Q_{k0} \{\cos[(\omega_k + \omega_0)t + \delta_k] + \cos[(\omega_k - \omega_0)t + \delta_k]\} \quad (2\text{-}3)$$

This expression shows that the dipole induced by monochromatic radiation emits polychromatic radiation. In this way, we get three types of radiation each one of them corresponding to different variations of frequency of the scattered radiation. The first term of the expression corresponds to Rayleigh elastic diffusion, having the same frequency as incident radiation. The second term is associated with Antistokes Raman diffusion that corresponds to the frequency $\omega_k+\omega_0$, and therefore related to a frequency increase compared to the incident radiation frequency. The last term represents Stokes diffusion occuring at $\omega_k-\omega_0$, which is inferior to incident radiation frequency[28].

Summarizing, one can affirms that Raman phenomena results from dipoles which oscillate at frequencies $\omega_0 \pm \omega_k$. These dipoles are originated by the modulation of the induced electric dipoles oscillating at the frequency of the incident field, through the vibration normal modes. The coupling of the electric field and the nuclear movement is ensured by the electrons, the rearrangement of which together with nuclear movement, imposes a harmonic variation of polarizability[28].

Figure 2-1 represents the Raman diffusion classic model, as well as an example of Raman diffusion in Potassium Selenate, studied by Tritt-Goc *et al.*[30], as a function of the temperature.

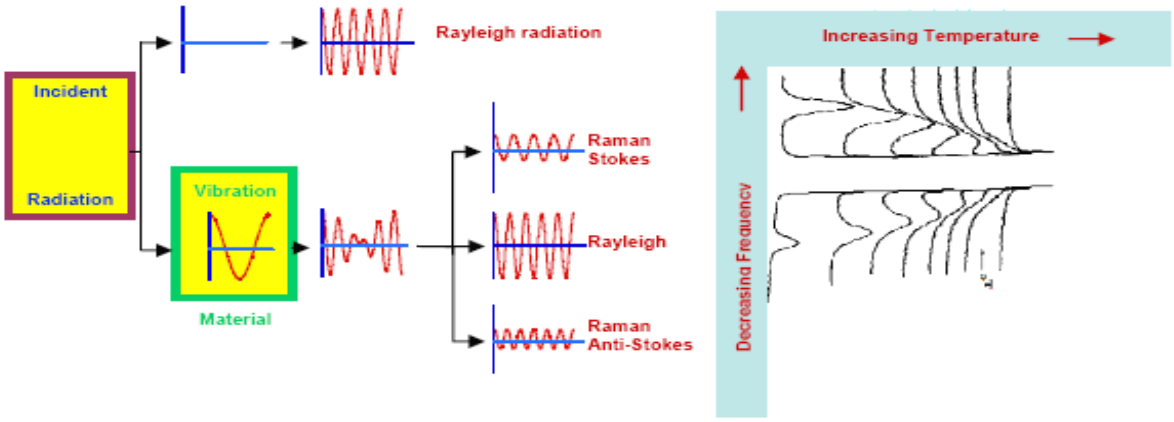

Figure 2-21 Classic model of diffusion and temperature dependence of Raman spectra in Potassium Selenate (adapted)[29].

Regarding equation 2-3, it is immediately perceivable that to obtain Raman spectra a non zero $(\alpha_{ij}^{`})_k$ is necessary. This classic selection rule constitutes a general method for the analysis of Raman activity in the vibration of normal modes of the system. However, this methodology is only applicable for simple molecules. This classic description becomes manifestly insufficient with increased molecular complexity. Consequently, a more complex treatment as suggested by quantum fundaments should be implemented[28].

2.1.2 Semiclassic description of Raman diffusion

The semiclassic description of Raman diffusion considers only the quantum details of the system in study. According to this approach, a transition between two levels is observed in the system, accompanied by absorption or emission of energy. Whenever a non-zero transition moment is present, it can be represented by the integral, which involves the wave functions of the initial and final states and the induced dipole moment operator:

$$\vec{P}_{fi} = \langle \psi_f | \vec{P} | \psi_i \rangle$$

The induced dipole moment operator $\vec{P}$ and the wave functions of the final and initial states are molecular coordinates and time dependent.

Let one considers only the amplitude of the transition moment for Raman intensity determination, since frequency dependence has already been analyzed in the classic theory.

By introducing the linear approach of the induced dipole moment, the following expression is obtained:

$$\left[\vec{P}_0\right]_{fi} = \left\langle \psi_f \left| \vec{\vec{\alpha}} \right| \psi_i \right\rangle \vec{E}_0$$

where $\left\langle \psi_f \left| \vec{\vec{\alpha}} \right| \psi_i \right\rangle$ represents the transition polarizability tensor.

The amplitude of incident radiation electric field can be placed outside of the integral as in Raman diffusion it is practically independent of the spatial coordinates. This fact results from the wavelength of the incident radiation electric field, which is superior to the dimensions of the unit cell. Hence, we can affirm that in Raman spectroscopy only those normal modes that are located at the centre of the Brillouin zone are observed.

By expanding the transition polarizability tensor in the normal coordinates of the vibration system to the first order, and considering only one mode of vibration Q, one obtains the expression

$$\left\langle \psi_f \left| \vec{\vec{\alpha}} \right| \psi_i \right\rangle = \vec{\vec{\alpha}}_0 \Big|_{Q=0} \left\langle \psi_f \left| \psi_i \right\rangle + \left(\frac{\partial \vec{\vec{\alpha}}}{\partial Q} \right) \right|_{Q=0} \left\langle \psi_f \left| Q \right| \psi_i \right\rangle + \ldots$$

Considering the development of wave functions in terms of the wave functions of the harmonic oscillator and the corresponding orthogonality properties, we can advance the conditions for the existence of Raman activity in the following way:

i. The first term corresponds to Rayleigh elastic diffusion. Due to orthogonality of the wave functions of the harmonic oscillator, this term is different from zero if i=f.

ii. The second term, involving the derived polarizability tensor, is only different from zero in the two following situations:

$$b_v (v_i + 1)^{1/2} \left(\frac{\partial \vec{\vec{\alpha}}}{\partial Q} \right) \Big|_{Q=0}, \quad \text{if } v_f = v_i + 1$$

$$b_v(\nu_i)^{1/2}\left(\frac{\partial\vec{\alpha}}{\partial Q}\right)\Big|_{Q=0}, \quad \text{if } \nu_f = \nu_i - 1$$

ν_i and ν_f are the quantum numbers of the initial and final states, respectively.

It was observed that only the vibration modes are active in Raman diffusion when the quantum number of the initial state of a unit varies. The first expression corresponds to the increasing of a unit and therefore to the creation of a phonon. It therefore represents Stokes diffusion. The second expression corresponds to the reduction of a unit and therefore to the absorption of a phonon. It represents AntiStokes diffusion[28].

The variation by a unit of initial state quantum number is a required condition. It is also indispensable to have at least one of the elements of the derived polarizability tensor different of zero.

The terms (υ_i+1) and υ_i show that the intensity of the Stokes diffusion is greater than that of Antistokes diffusion.

Using the Boltzman distribution law and adding over all the possible states, the expression for the rate of the Stokes and Antistokes intensities is:

$$\frac{I_{Stokes}}{I_{Antistokes}} \propto e^{\left(\frac{h\nu}{k_B T}\right)}$$

where υ is the vibration normal mode frequency, T the absolute temperature and k_B the Boltzmann constant.

This rate depends strongly on the vibration mode frequency and the temperature: it increases with the increasing of the frequency and with the decreasing of the temperature, in perfect agreement with the spectra presented above in the particular case of the Potassium Selenate.

The difference is lower at low temperatures since the excitation of Antistokes bands involves the absorption of a phonon which is thermically excited and later absorbed. On the other hand, Stokes band corresponds to the creation of a phonon and remains finite for T=0 K.

2.2 Experimental set-up

The facility used for obtaining Raman spectra is built by a laser system, a spectrometer T64000 Jobin-Ivon, two detection systems, a system of control and automatic data acquisition, as well as low temperature equipment (Figure 2-2).

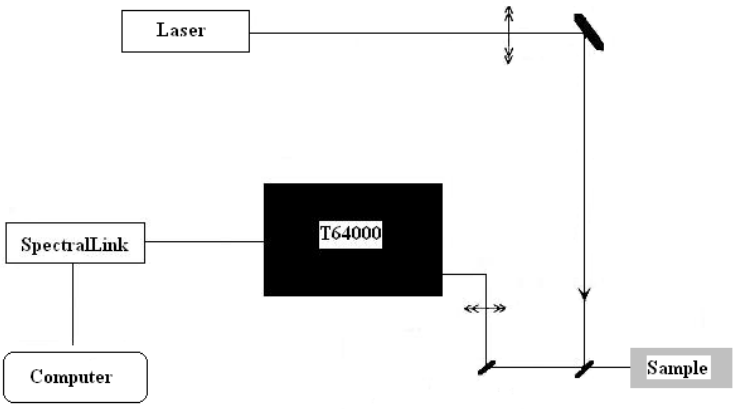

Figure 2-2 Equipment used for Raman measurements.

The incident radiation in the sample originates from an argon laser that emits continuous vertically polarised radiation in the green line wavelength (λ=514,53 nm). The emitted radiation presents a power gain and a signal/noise rate better than other lines in the electromagnetic visible spectrum. To avoid degradation and auto-heating of the sample, laser power has been chosen below 300 mW.

The study of Raman scattering as a function of temperature was carried out by using a closed cycle helium cryostat, in the temperature range 10-300 K. The sample was placed inside a copper cylinder that allowed performing measurements at the right-angle scattering geometry. To improve the temperature homogenization, a second copper mask was used as already referred above. A low temperature system allowed a temperature stability of 0.5 K with an accuracy of 0.1 K.

2.3 Raman spectra analysis

The frequency, width and intensity of Raman modes have been determined, by fitting a model of Independent Damped Harmonic Oscillators (IDHO), to the experimental data[30]. The intensity of the spectrum is then given by the following expression:

$$I(\omega,T) = [1+n(\omega,T)]\left[\sum_{j=i}^{N} A_{0j}\frac{\omega\Omega_{0j}^2\Gamma_{0j}}{(\Omega_{0j}^2-\omega^2)^2+(\omega\Gamma_{0j})^2}\right] \quad (2\text{-}4)$$

where $n(\omega,T)$ is the Bose-Einstein factor and, A_{0j}, Ω_{0j}, Γ_{0j} are the amplitude, frequency and damping of the *j* oscillator, respectively.

During the fitting procedure, Raman spectra have not been reduced. Thus an adequate temperature factor has been added to the expression 2-4. Moreover a Gauss function has been also included in 2-4, whenever the Rayleigh band had to be considered in the fitting procedure.

In order to gain a better understanding of the temperature behaviour in the first order Raman modes regarding their frequency, intensity and width, the expression 2-4 have been fitted to the Raman spectra for every measured temperature. An example of such a fitting is presented in Figure 2-3.

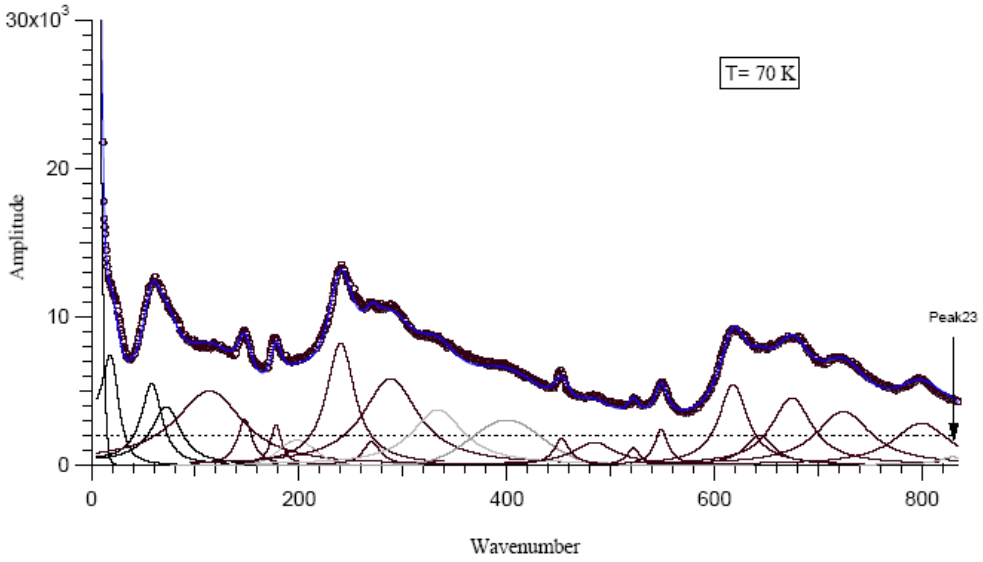

Figure 2-3 Example of IDHO fitting.

Figure 2-3 represents the IDHO fitting of Raman spectra for Y-doped $SrTiO_3$ at 70K. The spectrum was not reduced in temperature and the appropriate temperature factor included in the fitting function. Darker lines show first order bands, while the second order background and laser plasma lines are displayed by grey lines. A baseline was also included in the fitting function.

The ensuing sections describe the results obtained by IDHO analysis of La- and Y-doped $SrTiO_3$ ceramics Raman spectra. A detailed description will be provided so as to understand the lattice dynamics of doped $SrTiO_3$.

2.4 Lattice Dynamics and structural instabilities of $Sr_{1-1.5x}La_xTiO_3$ ceramics

The unpolarised Raman spectra of $Sr_{1-1.5}xLa_xTiO_3$ ceramics with x=0.01, at different fixed temperatures, is shown in Figure 2-4. As in undoped $SrTiO_3$ ceramics, second order features dominate the spectra at high temperatures. With decreasing temperature, however, the spectra present extra Raman-forbidden infrared active modes that stem from the local loss of their centro-symmetry, apparently associated with the granular micro-nanostructure of the samples.

The different modes in La-doped $SrTiO_3$ were identified by comparing the obtained data for x=0.01 with those reported in literature for nominally pure $SrTiO_3$[9,10] and for La-doped $SrTiO_3$ with x=0.05[11]. The study of such modes as a function of temperature is crucial to understand the dynamics of the doped $SrTiO_3$ lattice, particularly the origin of antiferrodistortive phase transition and quantum paraelectricity (Figure 2-5).

The next section will focus on the study of the antiferrodistortive phase transition concerning the underlying optical phonons that become Raman active.

2.4.1 Para-Antiferrodistortive phase transition in $Sr_{1-1.5x}La_xTiO_3$ ceramics

Figure 2-5 shows the temperature dependence of the phonon frequencies for $Sr_{1-1.5x}La_xTiO_3$ ceramics with x=0.01, 0.05 and 0.1 ranging from 0 to 600 cm^{-1}. For all compositions, the activation of E_g+B_{1g} doublet hard mode at 450 cm^{-1}, in the low temperature range, provides evidence for the onset of the antiferrodistortive phase occurring at T_a= 138 K, 199 K and 255 K for x=0.01, 0.05 and 0.1, respectively.

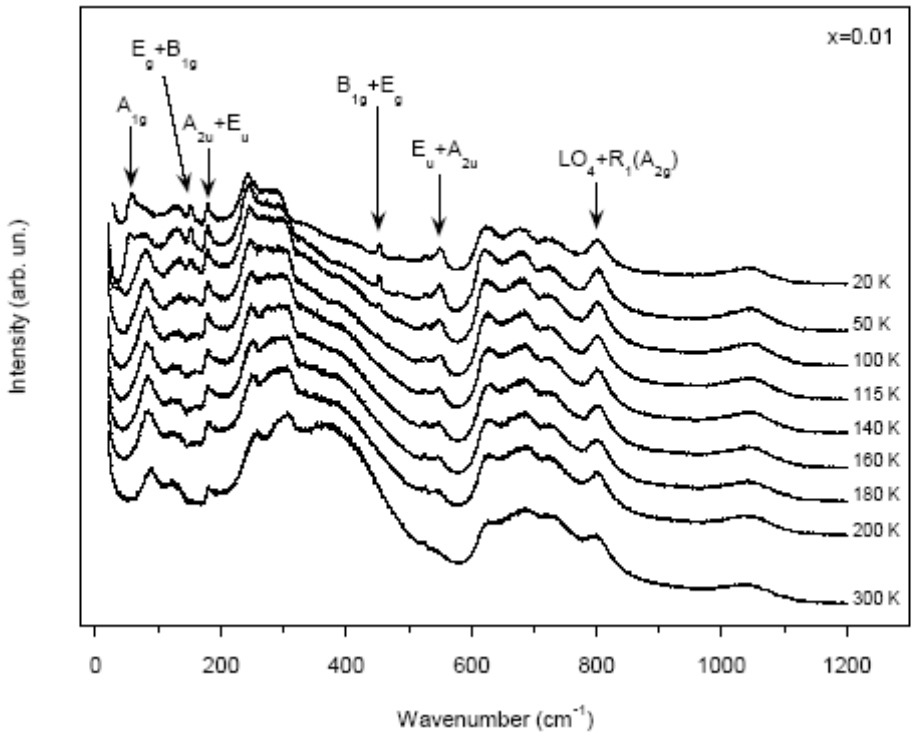

Figure 2-4 Temperature dependence of the Raman spectra for the x=0.01 La-doped $SrTiO_3$ ceramic in the 0-1200 cm^{-1} frequency range.

These results support preceding TEM observations that have remarked a relation between T_a and tolerance factor (*t*) for different $SrTiO_3$ dopants[20]. Actually, from TEM and Raman investigations it is found that T_a increases while Sr^{2+} substitution by ions with smaller ionic radius.

It is worth pointing out the main features of the behaviour of optical phonon frequencies below 100 cm^{-1}. Frequency behaviour of Raman modes in the lower frequency range is rather different from that observed in the higher frequency range (see Figure 2-5). Here one can found, for all Lanthanum compositions, the A_{1g} soft mode associated with the octahedral tilting (see Figure 2-6), the driving mechanism of antiferrodistortive phase transition. However, A_{1g} softening could not be ever observed for x=0.1. Due to its high importance in lattice dynamics of related $SrTiO_3$ systems, the frequency of the A_{1g} mode was studied as a function of the temperature.

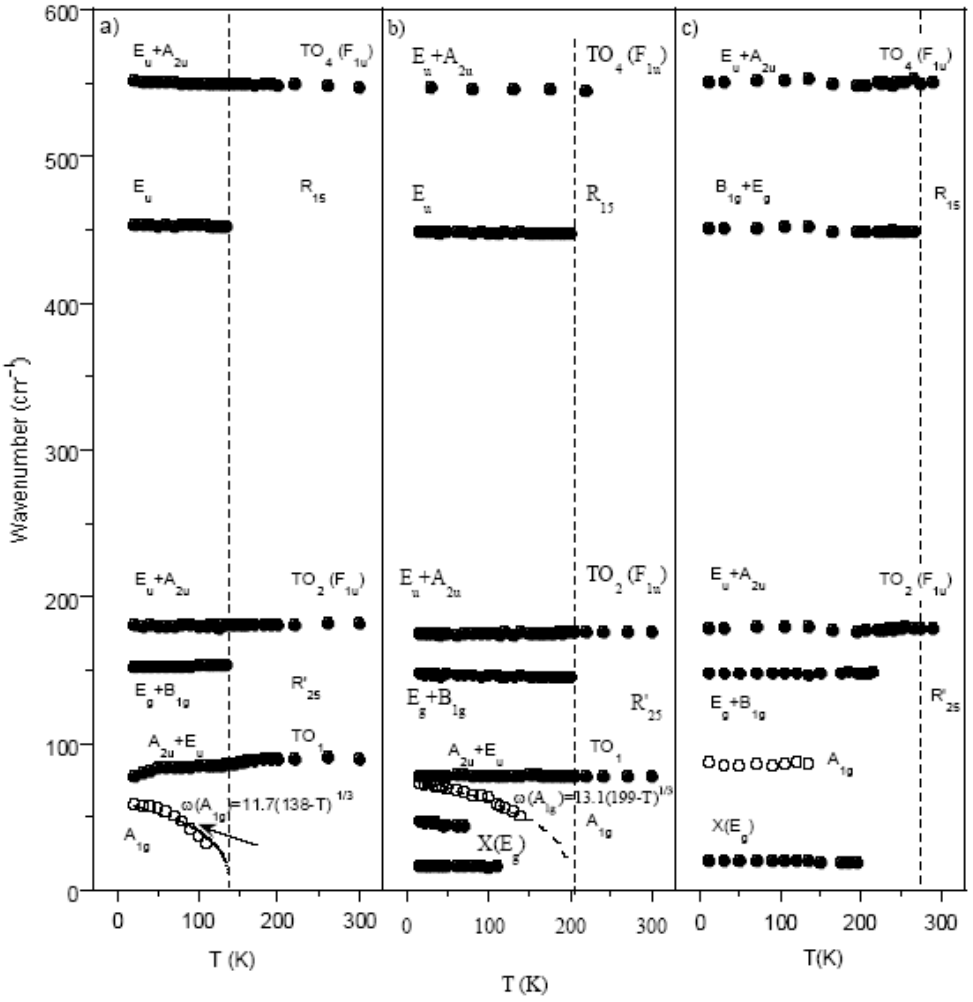

Figure 2-5 Frequency variation of the first order Raman modes with temperature, for a) x=0.01, b) 0.05 and c) 0.1 in the 0-600 cm^{-1} frequency range.

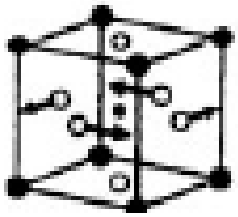

Figure 2-6 A_{1g} (R-point) vibrational mode.

From the classical Cochran softening law, $\omega_{A1g}=K(T_a-T)^{\beta}$, one can compute K, T_a and β as fitting constants[11]. For x=0.01, K=11.7 $s^{-1}K^3$, T_a=138 K, and β=1/3 were obtained,

while for x=0.05 the attained values are K=13.1 $s^{-1}K^3$, T_a=199 K and, β=1/3. The β values are quite similar to those of undoped $SrTiO_3$ ceramics[9] and thoroughly agree with the results of the model put forward by Petzelt *et al.*[9]. Moreover, T_a temperature values obtained by the fitting procedure are also quite close to those determined from the activation of the R-point modes. It is very interesting to see that, for x=0.05, the A_{1g} mode undergoes a 'hardening' process associated with the increase of Lanthanum content. These results corroborate the idea that Lanthanum change the elastic properties of $SrTiO_3$ ceramics considerably.

The band at ~50 cm^{-1} only observed for x=0.05 Lanthanum content, is assigned to an E_g mode. The E_g hardening relating to the pure single $SrTiO_3$ crystal can be attributed to its coupling with the mode close to ~20 cm^{-1} (LF-mode)[10]. This mode is also detected in x=0.1. The fact that this mode is only observed for higher concentrations of Lanthanum might be an indication that the LF-mode is a defect-induced Raman mode[11]. Figure 2-7 shows the x-dependence of the para-antiferrodistortive phase transition temperatures T_a.

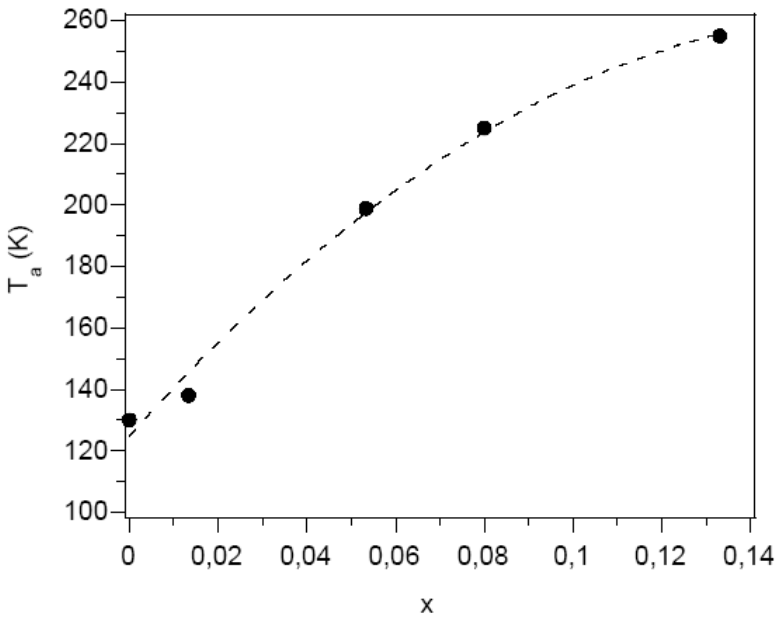

Figure 2-7 Para-antiferrodistorsive phase transition temperature, T_a, as a function of Lanthanum concentration, x.

The T_a shift has been associated with internal elastic changes due to the inclusion of Lantahanum in pure $SrTiO_3$ that leads to a more favourable tilting of the oxygen tetrahedral, thereby pushing T_a towards high temperature ranges. This feature spans over more than 120 K, in accordance with the TEM results[20].

2.4.2 Quantum paraelectricity in $Sr_{1-1.5x}La_xTiO_3$ ceramics.

It has been observed in the $SrTiO_3$ system that, in the low temperature range, TO1 mode is either polarized in *ab*-plane, E_u, or along *c*-axis, A_{2u}, but does not totally soften due to quantum fluctuations[8]. For $Sr_{1-1.5x}La_xTiO_3$, the TO1 optical mode does not appear for all the compositions studied. In fact, TO1 is not visible in the highest Lanthanum concentration ceramic, x=0.1. As in undoped $SrTiO_3$, this mode does not reach zero frequency. Therefore, a ferroelectric state is never expected at low temperatures, which is in rather good agreement with data reported in literature[13].

It is believed that in addition to quantum fluctuations, tetragonal distortion of oxygen octahedral is an essential mechanism to prevent the ferroelectric transition in $SrTiO_3$ related materials[31] which was recently confirmed by TEM[20].

2.5 Lattice Dynamics and structural instabilities of $Sr_{1-1.5x}Y_xTiO_3$ ceramics

Figure 2-8 illustrates unpolarised Raman spectra for $SrTiO_3$ and for x=0.005, 0.01 Y-doped $SrTiO_3$ ceramics, in the frequency range 5-1000 cm^{-1}, at room temperature. As well as for La-doped $SrTiO_3$ ceramics, Yttrium doping leads to the rise of a number of new bands in the Raman spectra, which is strongly affected by second order scattering.

$Sr_{1-1.5x}Y_xTiO_3$ ceramics Raman spectra were investigated at different temperatures (see Figure 2-9) regarding phonon frequencies determined for x=0.005 (Figure 2-9 a)), x=0.01 (Figure 2-9 b)), ranging from 0 to 600 cm^{-1}.

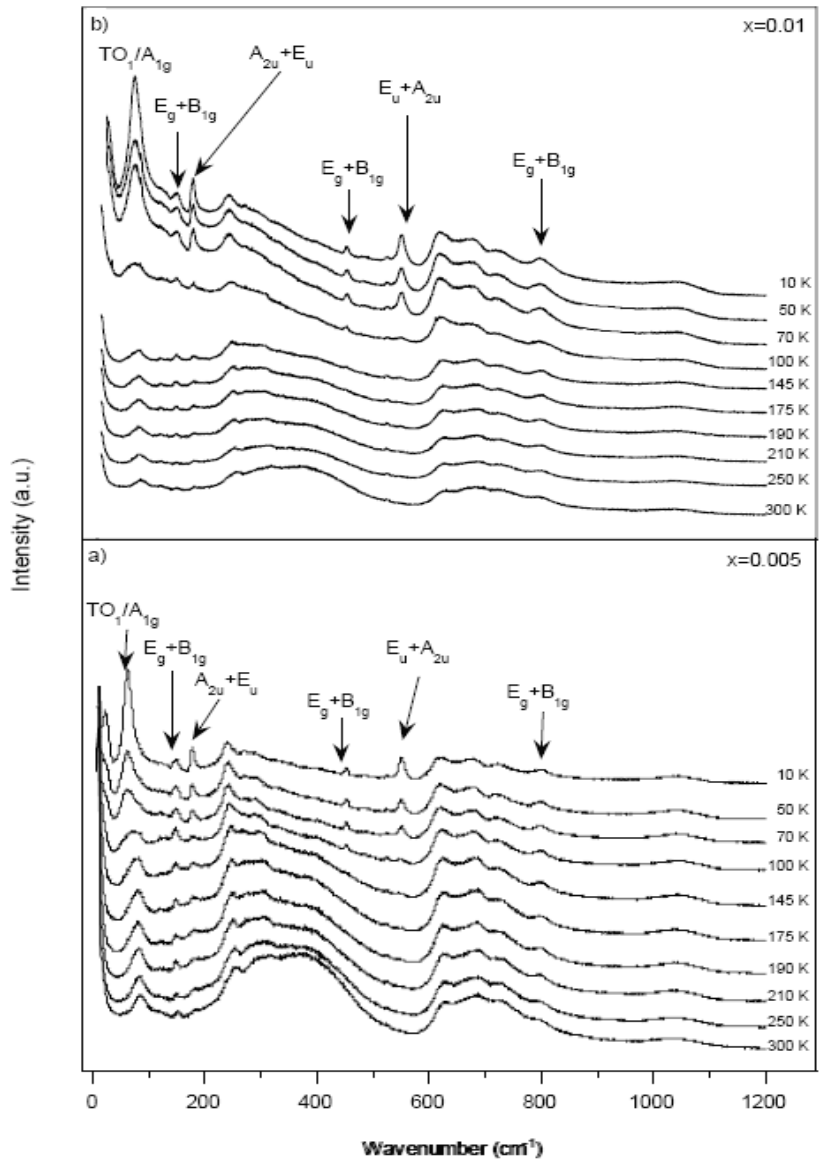

Figure 2-8 Raman spectra for x=0.05 and 0.1, at different temperatures.

2.5.1 Para-Antiferrodistortive phase transition in $Sr_{1-1.5x}Y_xTiO_3$ ceramics

The behaviour of the modes between 100 and 600 cm^{-1} is quite similar to that of La-doped $SrTiO_3$ ceramics (see Figure 2-9). Also, in this system, Raman activation of hard modes, E_g+B_{1g}, marks the para-antiferrodistortive phase transition at 165 K, and 195 K for x=0.005 and 0.01, respectively. Similarly to $SrTiO_3$ and La-doped $SrTiO_3$, in Y-doped $SrTiO_3$ the softening of the A_{1g} vibrational mode is observed as well. The

Cochran law fitting of A_{1g} mode revealed a similar K and β parameters to the ones obtained in La-doped $SrTiO_3$, although a greater shift towards higher temperatures was observed (see Figure 2-5 and 2-8). Besides, the activation of hard modes at 450 cm^{-1} completely corroborates with T_a found by Cochran analyse. The predictions of T_a increase while *t* decreases is confirmed in this system.

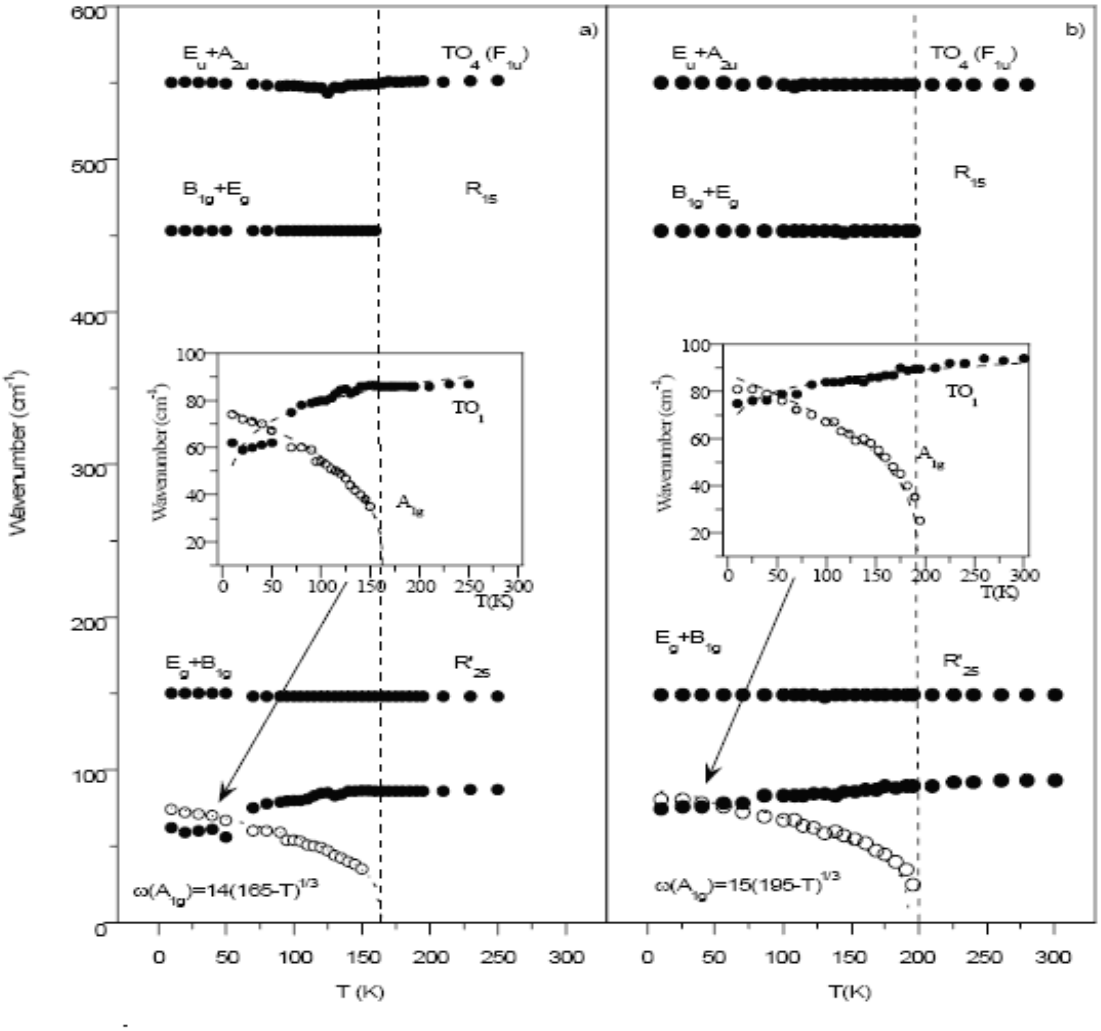

Figure 2-9 Frequency variation of the first order Raman modes with temperature, for a) x=0.005, b) 0.01 in the 0-600 cm^{-1} frequency range.

2.5.2 Quantum paraelectricity in $Sr_{1-1.5x}Y_xTiO_3$ ceramics

Previous works addressed to the study of $Sr_{1-1.5x}Y_xTiO_3$ ceramics dielectric behavior, have exposed the non existence of a ferroelectric phase in this system. However,

dielectric anomaly at low temperatures was reported by the same authors though it is still not clear. The obtained Raman spectra for $Sr_{1-1.5x}Y_xTiO_3$ ceramics reveal the existence of polar TO1 mode at low temperatures which does not totally soften for both studied compositions. Hence, it can be confirmed that Yttrium incorporation in SrTiO3 lattice does not induce a ferroelectric state.

2.5.3 Discussion and Conclusion

In order to understand the influence of the type of dopant in $SrTiO_3$ lattice dynamics, the Raman spectra of $Sr_{1-1.5x}La_xTiO_3$ and $Sr_{1-1.5x}Y_xTiO_3$ (x=0.01) ceramics will be compared between each other and to undoped $SrTiO_3$.

Raman spectra of undoped and La-and Y-doped $SrTiO_3$ systems shown in Figure 2-10, reveal similar behaviour, except in the low frequency range, where differences in the position, intensity, and width of some bands are clearly observed.

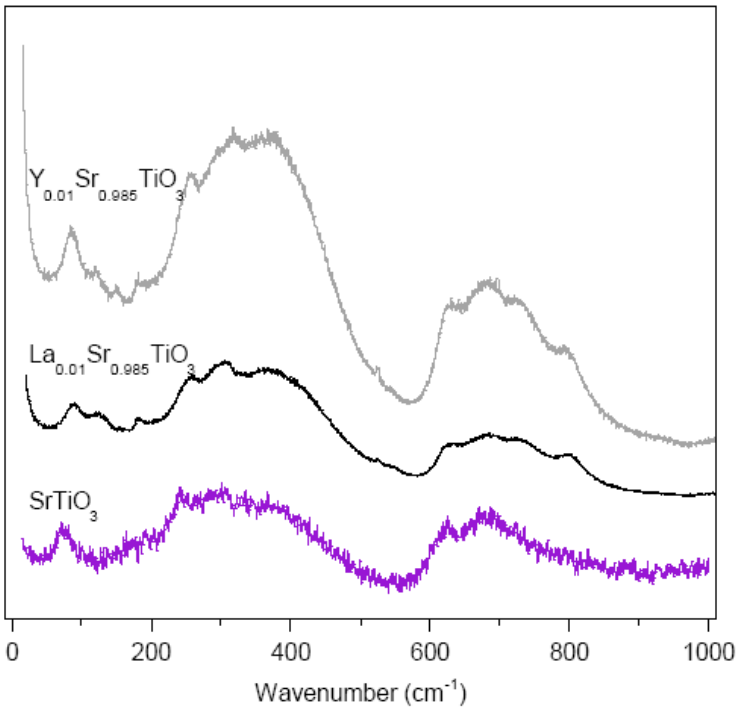

Figure 2-10 Raman spectra for pure $SrTiO_3$, $Sr_{0.985}La_{0.01}TiO_3$ and $Sr_{0.985}Y_{0.01}TiO_3$ ceramics, at room temperature.

Furthermore, the temperature dependence of Raman modes between 100 and 850 cm^{-1} is quite alike irrespectively of impurity type. The activation of both E_g and B_{1g} R-point hard modes in the low temperature range clearly marks the para-antiferrodistortive phase occurring at 138 K and 195 K, for Lanthanum and Yttrium, respectively. Thus, T_a is seen to be strongly dependent on the type of dopant used and of *t* . Before a discussion of the actual origin of this dependence, it is worth mentioning main features of the thermal behaviour of optical phonons frequencies below 100 cm^{-1}, which are rather different from the one observed in the higher frequency range.

The A_{1g} mode, the softening of which has been linked with octahedral tilt, is observed for both doped systems. Table 2-1 summarizes the constants obtained for undoped and doped $SrTiO_3$ ceramics, through Cochran law fitting.

System	K($s^{-1}K^3$)	T_a	β
$SrTiO_3$ [9]	11.2	132	1/3
$Sr_{0.985}$ $La_{0.01}TiO_3$	11.7	138	1/3
$Sr_{0.985}$ $Y_{0.01}TiO_3$	15	195	1/3

Table 2-1 Cochran law constants for $SrTiO_3$, $Sr_{0.985}$ $La_{0.01}TiO_3$ and$Sr_{0.985}$ $Y_{0.01}TiO_3$ ceramics.

It had been thought that T_a decreases with the increasing of the lattice parameter, until it was reported that T_a of Mg,- and Nb-$SrTiO_3$ increases with the lattice parameter[26]. To explain such phenomena, several authors have pointed out that T_a may be not dependent on lattice paramenter but rather on the tolerance factor, *t*,

$$t = \frac{r_A + r_O}{\sqrt{2}(r_B + r_O)}$$

where r_A , r_B and r_O are the ionic radii of A-, B- and oxygen sites, respectively. In accordance with this model, T_a decreases when *t* increases, and vice-versa. Thus, Sr^{2+}substitution leads to an increasing of T_a for dopants with an ionic radius lesser than that of the one of Sr^{2+}, since in this case, *t* decreases. The opposite is observed for dopants with radii greater than that of Sr^{2+}. For substitution located at the Ti^{4+} lattice

site, an inverse rule is applicable, as the ionic radius of the dopant is placed at the denominator of *t*. Figure 2-11 shows an assembly of a number of previous results concerning the T_a of dopants substituting either Sr^{2+} or Ti^{4+} sites[26]. Ba^{2+}, Pb^{2+}, Ca^{2+}, La^{3+}, Mn^{2+} ions replace the Sr^{2+} site due to a similar ionic radius. For such dopants, following the rule referred to above, T_a decreases. This is due to the lesser radii of those dopants, which leads to an increase of *t*. Conversely, for Mn^{4+}, Mg^{2+}-Nb^{5+} and Mg^{2+} doping, placed at the Ti^{4+} site, T_a increases. In addition, the increasing of dopant concentration for either site leads to a larger absolute shift of T_a, due larger corresponding changes of *t*[26].

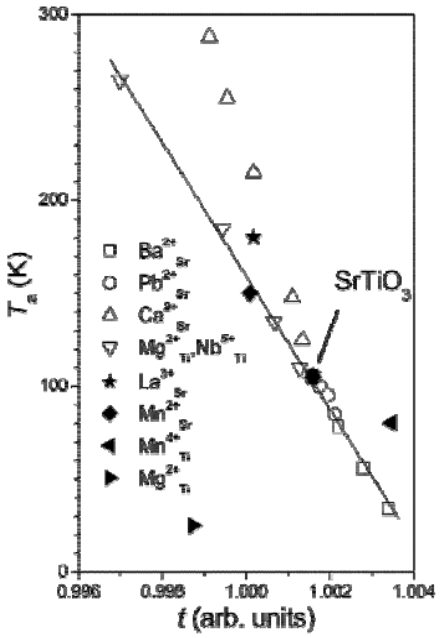

Figure 2-11 Para-antiferrodistortive phase transition temperature, T_a, for undoped and doped $SrTiO_3$ as a function of the tolerance factor *t*[26].

In this work it is aimed to study this type of behaviour in Y- and La-doped $SrTiO_3$ ceramics. If one assumes, from the chemical and structural results obtained, that doping is most likely to occur at the A-site of the lattice and its coordination number being 12 the *t* values are displayed in Table 2-2 together with the corresponding T_a. The ionic radii values for Sr^{2+} and Ti^{4+} ions are also included for comparison.

	r_A	*t*	T_a (K)
Y^{3+}	1.25	0.95	195
La^{3+}	1.37	0.99	138
Sr^{2+}	1.44	1.00	132
Ti^{4+}	0.610	-	-

Table 2-2 Ionic radius and T_a.

Thus, it has been confirmed that Y^{3+} is characterized by a lower *t* value than La^{3+} and so by a higher T_a. A straightforward correlation between tolerance factor *t* and T_a values does in fact exist in these systems.

3 Thermally Stimulated Currents (TSC) in $Sr_{1-1.5x}La_xTiO_3$, $Sr_{1-1.5x}Y_xTiO_3$, $Sr_{1-x}Mn_xTiO3$ and $SrTi_{1-y}Mn_yO_3$

Thermally Stimulated Currents (TSC) is a very powerful and efficient method to identify and characterize relaxation processes in dielectrics. In this chapter, TSC of some doped $SrTiO_3$ ceramics will be analysed regarding the nature of their polar mechanisms. The theory and experimental details of TSC is presented in section 3.1. This is followed by the experimental results obtained in La-, Y- and Mn-doped $SrTiO_3$ ceramics and their discussion by employing theoretical models.

3.1 Theory and Experiments

3.1.1 Dielectric Relaxation in Solids

It is of the general knowledge that dielectrics are insulators and supporters of electrostatic fields. When submitted to an external electrical field may evidence various types of electrical polarisation[31]:

a. Atomic polarisation: that takes place whenever displacement of atoms occurs in molecules with heteropolar bonds;
b. Electronic polarisation: originated by the deformation of the electronic shell;
c. Dipolar polarisation: associated with the existence of molecular or ionic dipoles;
d. Space-charge polarisation: due to the migration of existent free charges to electrodes;
e. Interfacial or Maxwell-Wagner-Sillars polarisation, which is attributed to the formation of charged layers at interfaces;
f. Creation of free charges by injection process from electrodes during the application of high electrical fields.

Dielectric relaxation results from the polar response of a dielectric to an external electric field, often at both radio and microwave frequencies. Dielectric mechanisms are mostly identified in terms of permittivity as a function of frequency and can often be described either by the Debye model itself or other slightly modified Debye models[33].

3.1.2 Bucci-Fiesci Theory

The charging and discharging currents of the ordinary dielectric capacitor occurring for times higher than 10^{-12} s are in general related to orientational (or dipolar), interfacial or space charge polarisation. In agreement with the Bucci-Fiesci theory, dipoles` reorientation, due to both electrical field and their random thermal motion, compete with each other, thereby inducing dipolar polarisation. In other words, dipoles` reorientation due to electrical fields is strongly disturbed by thermal noise.

Let one now find the expression for the Thermally Stimulated Depolarisation Current (TSDC). Assuming a Debye model, the polarisation in a unit volume under an external electric field F_p, during time *t* and at temperature T_p is described by the following expression:

$$P(t) = P_e\left[1 - \exp\left(\frac{-t}{\tau}\right)\right] \quad (3\text{-}1)$$

In the above expression τ is the dipolar relaxation time and P_e the equilibrium polarisation given by Langevin equation 3-1:

$$P_e = \frac{sN_d p_\mu^2 \kappa F_p}{kT_p} \quad (3\text{-}2)$$

where *s* is a geometrical factor, N_d the dipole concentration, p_μ dipole electrical moments, *k* Boltzmann´s constant and κF_p the local electric field.

After removing the field at t=∞, the time dependence of polarisation may be described as:

$$P(t) = P_e \exp\left(-\frac{t}{\tau}\right) \quad (3\text{-}3)$$

Considering the equation 3-3, depolarisation current density may be expressed as:

$$J(t) = -\frac{dP(t)}{dt} = \frac{P(t)}{\tau} \quad (3\text{-}4)$$

where it is assumed that:

i. The temperature increases linearly with time at a q rate, as $T=T_0+ qt$;

ii. Thermal dependence of relaxation time is described as:

$$\tau(T) = \tau_0 \exp\left(\frac{E}{kT}\right) \quad (3\text{-}5)$$

where τ_0 is the relaxation time at infinite temperature, and E is the activation energy.

iii. The initial frozen-in polarisation, $P(T_0)$ is equal to $P_e(T_p)$.

The depolarisation current density (J_D) current is then described as:

$$J_D(T) = \frac{P_e(T)}{\tau_0} \exp\left(-\frac{E}{kT}\right) \exp\left[-\frac{1}{q\tau_0} \int_{T_0}^{T} \exp\left(-\frac{E}{kT}\right) dT'\right] \quad (3\text{-}6)$$

This expression proved to be very useful in analysing the experimental Thermally Stimulated Depolarization Currents (TSDC) data as permit to obtain the electric polarisation, activation energy and relaxation time associated with the dipolar relaxation mechanism. The first exponential, which dominates in the low temperature range, is responsible for the initial increase of the current with the temperature, while the second exponential which dominates at higher temperature, gradually slows down the current rise and then depresses it very rapidly.

By differentiating 3-6, the temperature T_m of the maximum of the TSD current peak can be analytically determined as:

$$T_m = \left[\frac{E}{k} q\tau_0 \exp\left(\frac{E}{kT_m}\right)\right]^{1/2} \quad (3\text{-}7)$$

T_m is independent of the applied electric value used for sample polarisation.

Analytical solutions for the currents resulting from a space charge polarisation in structural heterogeneous materials revealed themselves to be rather complex, as approximations are required to obtain an analytical $J_D(T)$ function. In most real dielectrics the interfacial and space-charge polarisations cannot be separated and, consequently, it is only possible to present a qualitative analysis.

It have been identified a relaxor behaviour, at low temperatures, in some doped $SrTiO_3$ ceramics. Thus, from the application of TSC technique to the study of these ceramics the origin of such relaxation processes could be understood.

3.1.3 TSC experimental technique

The mechanisms often responsible for the discharge or depolarization of polarizable materials are either reorientation of dipoles or space charges` motion. During reorientation of dipoles, certain energy, known as activation energy, is required. Thus discharge due to dipole reorientation is a thermally-activated process. Furthermore, space charges commonly present in certain materials, like electrets, are kept immobilized near electrodes. During heating they start to move and become neutralized by recombination with charges of opposite sign. Figure 3-1 depicts the thermal dependence of poly (methyl, ethyl, ter. Butyl, and cyclohexyl) methacrylate discharge currents.

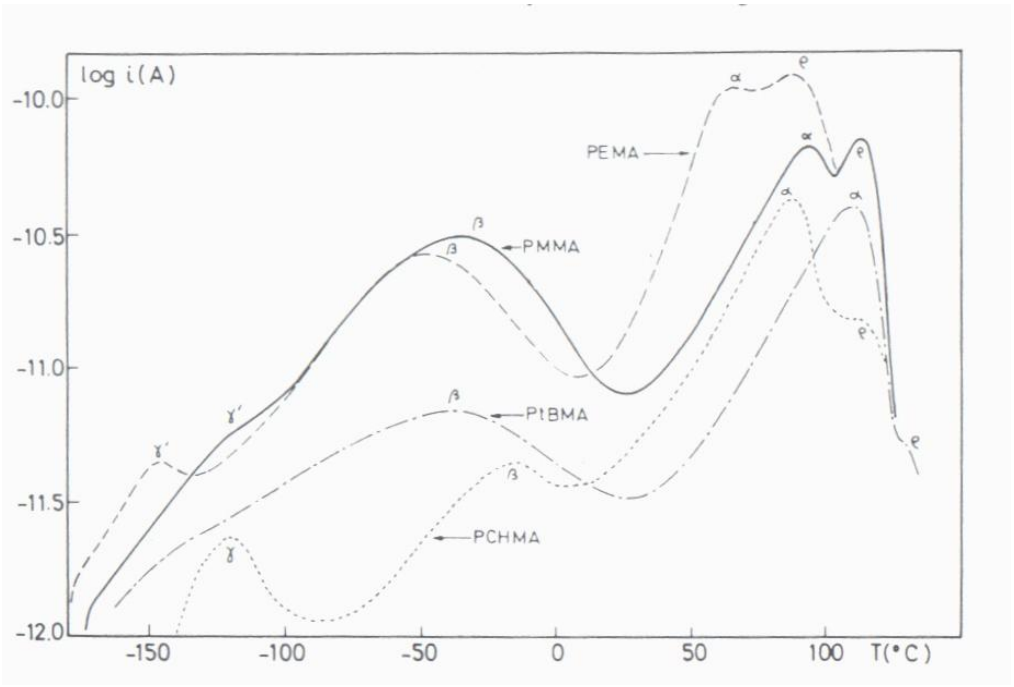

Figure 3-1 Current spectra of poly (methyl, ethyl, ter. Butyl, and cyclohexyl) methacrylate discharge currents[34].

One can observe space charge motion at high temperatures, associated with ρ current anomaly, whereas dipole reorientation mainly takes place at low temperatures. This is clearly revealed by both α and β current peaks shown in Figure 3-1. Unlike the reorientation of dipoles that only requires local rotation, the neutralization of space charges demands they move over several atomic distances.

Figure 3-2 shows the schematic representation of a thermally stimulated current experiment. The sample is polarized by an applied electric field at a temperature T_p, for a given time interval, t_p.

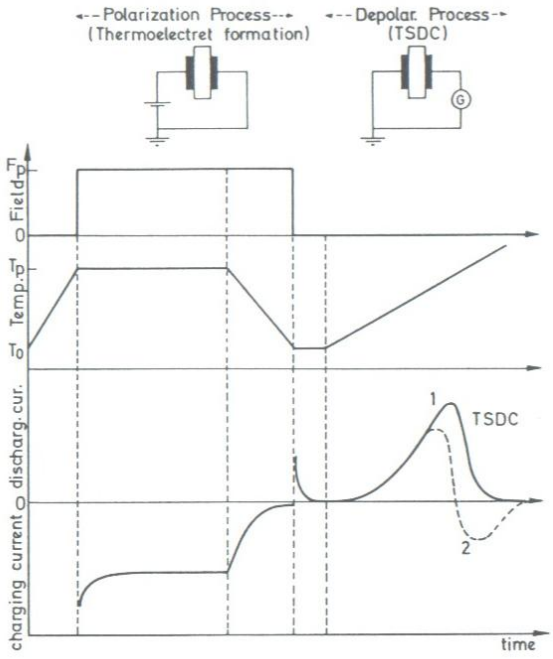

Figure 3-2 TSC experimental technique procedure[33].

In the presence of the electric field, the sample is cooled down to a temperature T_0 at rate q_1. The transition from a neutral to a polarized state produces thermally stimulated polarisation currents (TSPC) and thus a thermoelectret can be formed. After an isothermal time period and in the absence of the electric field, the sample is heated at rate q_2. The discharge mechanism gives rise to a current (TSDC, Thermally Stimulated Depolarization Current), which firstly increases with increasing temperature, and then decays when the supply of charges is depleted.

Free charges from interface dielectric-electrode may be also released, thereby contributing to TSD currents when a normal TSD circuit is used (Figure 3-3 a)). Several authors have proposed different set-ups considering that the release of interfacial charges may be avoided in a circuit with an air gap or in an open circuit (Figure 3-3 b) and c), respectively.

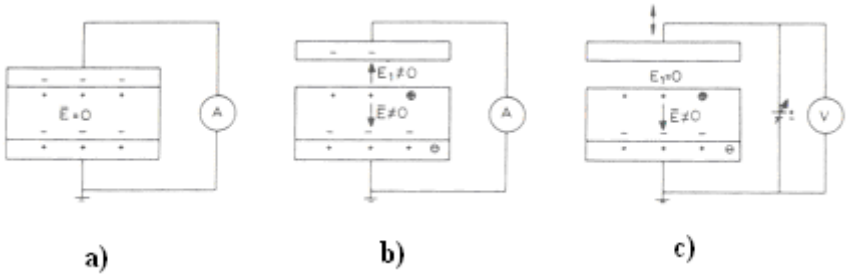

Figure 3-3 a) Normal TSD circuit, b) TSD circuit with an air gap, and c) charge TSD in open circuit[34].

3.2 TSC experimental set-up

The study of thermally stimulated currents was carried out in sequential thermal cycles as follows: i) Zero Field Cooling (ZFC)- the ceramic was first cooled down from room temperature to 10 K; ii) Field Heating (FH)- the sample was polarized with a d.c. field while heated from 10 K to room temperature; iii) Field cooling (FC) – the polarized ceramic was cooled down to 10 K and finally, iv) Zero field heating (ZFH)– the sample was then heated. The sample is short-circuited with a resistance 10^8 Ω (which is two to four orders of magnitude lesser than the sample resistance) in order to neglect leakage currents. For TSDC analysis, only ZFH currents in the temperature range of 10-300 K were considered.

Figure 3-4 illustrates the standard set-up for TSDC measurements. The potential difference across the resistance was detected with a Keithley 610C electrometer while keeping temperature rate of about 1K/min with a heater winding.

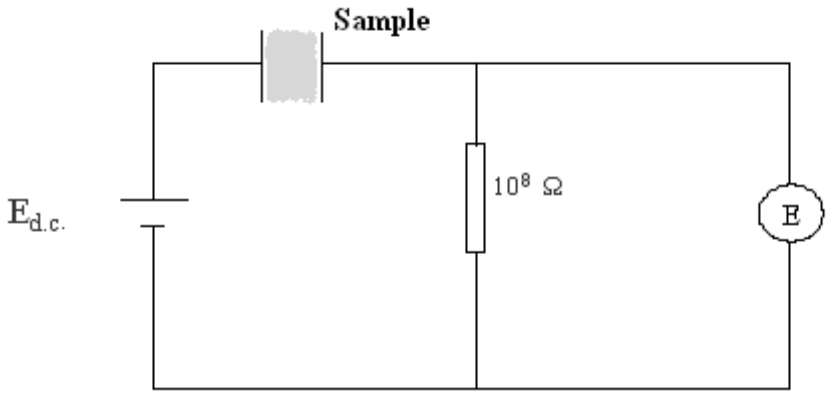

Figure 3-4 Standard short circuit to TSC measurements.

The sample temperature was measured with accuracy greater than 0.1 K and at high vacuum of 10^{-5} torr.

3.3 TSC of $Sr_{1-1.5x}La_xTiO_3$ ceramics

The results from thermal cycles measurements in $Sr_{1-1.5x}La_xTiO_3$ ceramics for x=0.01, 0.015 and 0.1 are summarized in Figure 3-5[11]. Sequential thermal cycles were carried out under an applied electrical field of 480 Vcm^{-1}. For all compositions, no ferroelectric behaviour is disclosed, as no zero field cooling (ZFC) current was detected. However, when an electric field is applied to ceramics, polar states are induced, revealed by anomalies in ZFH currents. Furthermore, electric current obtained in both FH and FC and ZFH and ZFC runs reveal that La-doped $SrTiO_3$ ceramics exhibit a strong non-ergodic behaviour clearly exposed by the different temperature behaviour of the obtained currents. Apparently, the history of the sample has a remarkable effect on its electrical properties.

As has been reported, in La-doped $SrTiO_3$ the bandgap decreases with increasing Lanthanum concentration[11]. Thus, La-doped $SrTiO_3$ can be regarded as a n-type semiconductor[11]. This is clear by the large electric current observed in the FH-FC runs at high temperatures[35] (see Figure 3-5).

Figure 3-6 shows the temperature dependence of TSDC and the corresponding polarisation P(T), in x=0.01, 0.05, and 0.1 samples, at different fixed magnitudes of the polarising electric field $E_{p.}$ The experimental results presented give clear evidence of different types of anomalies: anomaly I occuring around T_{mI}~80 K, and anomaly II observed around T_{mII}~170 K. The band structure observed below 50 K for x=0.01 is most probably the effect of a complex low-temperature, elastic-electrical domain configuration, which was previously observed in pure $SrTiO_3$[10,11]. A further broad anomaly (III) is observed for x=0.01 and 0.05. In the following section, we shall address only the results relative to anomaly I and anomaly II as anomaly III is very small in intensity which makes difficult a TSC analyse.

Figure 3-6 clearly reveals that anomaly I is quite dependent on Lanthanum concentration in regards to both its intensity and position. Figure 3-7 shows T_m position of anomaly I as a function of Lanthanum content with an average rate of ~3 K/%La.

The intensity, which is proportional to the area of the current peak, also increases for a fixed value of the polarizing field, when %La increases.

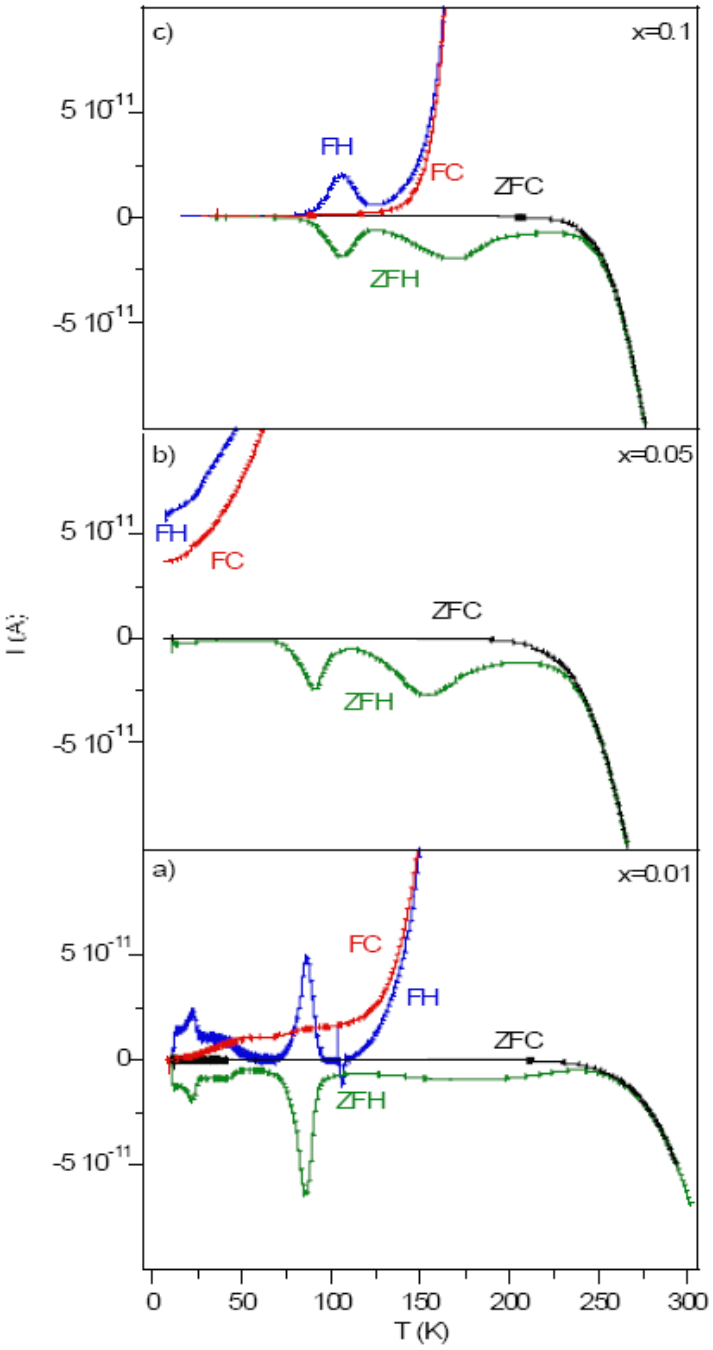

Figure 3-5 Temperature dependence of ZFC-FH-FC-ZFH electric currents under a field of 480 V/cm, for a) x=0.0133, b) x=0.05 and c) x=0.13

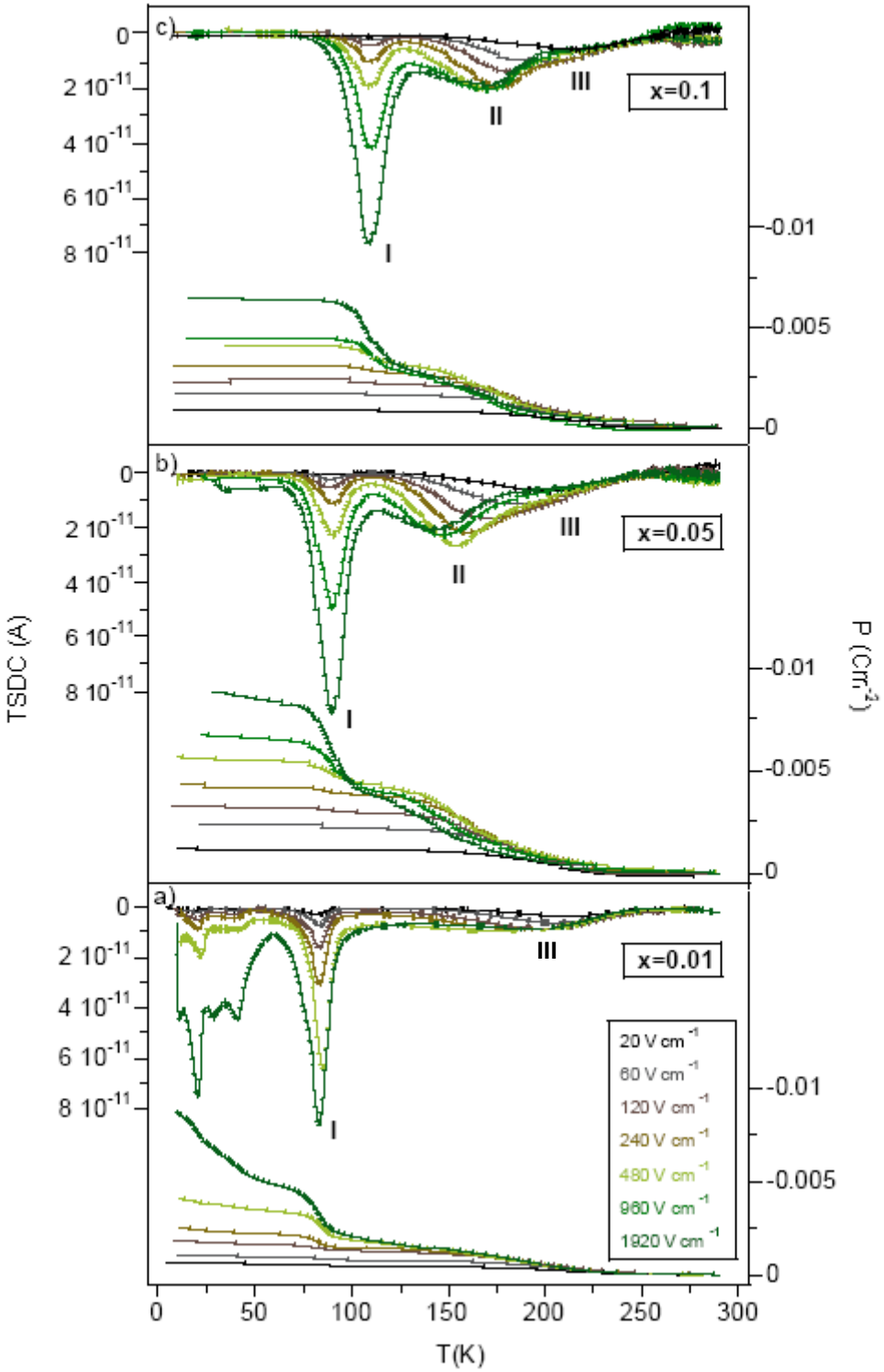

Figure 3-6 TSDC and corresponding polarization as a function of temperature at different fixed polarizing field E_p for a)x=0.01, b) x=0.05 and c) x=0.1.

For two of the ceramics with the highest dopant concentration, a new anomaly may occur at T> 200 K (anomaly III), which may be too small in intensity for x=0.1 or even non-existent. This feature is also a clear evidence of the importance of Lanthanum doping, mostly related to space-charge depolarization mechanisms. Such behaviour may be associated to the existence of oxygen vacancies at T> 100 K previously detected in dielectric spectra by Zhi *et al.* [13].

The saturation values of polarization give quite interesting results, which may indicate that this system should be a good candidate for technological applications, mainly as electrets, at least below liquid nitrogen temperatures. Unfortunately, a further increase of anomaly I maximum temperature, through increasing Lanthanum doping, may not be easy as it is quite difficult to process monophasic samples for higher lanthanum concentrations.

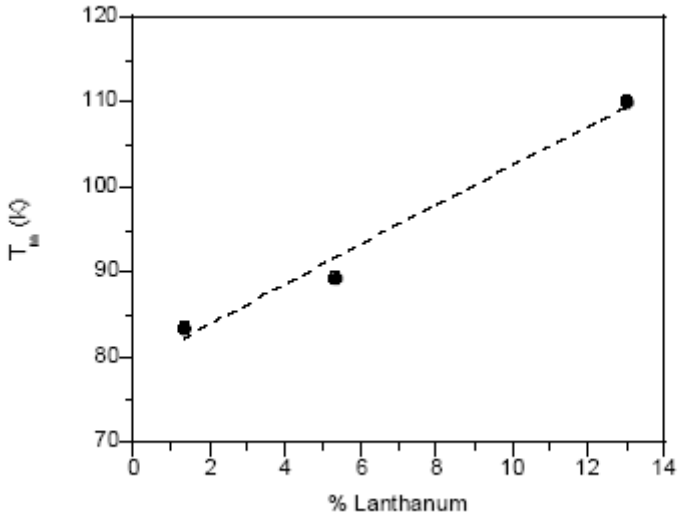

Figure 3-7 T_m vs %Lanthanum, for anomaly I.

In order to gain better knowledge of the nature of polar states revealed through thermally stimulated currents obtained for La-doped $SrTiO_3$ ceramics, a detailed analysis of the peak characteristics based on arguments given by Vanderschueren and Gasiot[33] was performed. According to these authors the field dependence of some peak characteristics can provide relevant information concerning the nature of their relaxation processes. One of the arguments for distinguishing relaxation processes, like dipolar

relaxation and space-charge relaxation, is based on the field dependence of thermally stimulated depolarization currents. TSDC peaks corresponding to dipole relaxation mechanisms are characterized by field-independent maximum amplitude temperatures, and by maximum amplitudes that are strictly proportional to the field strength. A different pattern is obtained from processes involving space-charge polarization, since generally the build-up, release and equilibrium spatial distribution of the charge are strongly dependent on the applied field.

Figure 3-8 illustrates the field dependence of the maximum amplitude of TSDC and Figure 3-9 the maximum amplitude temperature concerning anomaly I, II and III for x=0.01, 0.05 and 0.1. According to the theoretical predictions referred to above[33], we can state that anomaly I is most probably associated with a dipolar type relaxation process, as the linear behaviour of the maximum amplitude (Figure 3-8) and the invariance of the maximum amplitude temperature (Figure 3-9) versus the applied field clearly confirms. The corresponding parameters for anomaly II have a markedly different field-dependence, when compared to the anomaly I, revealing that anomaly II is probably due to a space-charge relaxation process. This assumption is strongly supported by the data shown in Figure 3-6, where we can observe just above ~100 K that the field-heating current becomes increasingly greater with increasing temperature. This behaviour is commonly associated with space charge depolarisation mechanisms, where bulk and surface charge displacements play a major role. This result is in good agreement with the one found in dielectric spectra in which oxygen vacancies dominates 100–300 K spectra range. Space-charge polarization is a much more complex phenomenon than dipolar polarisation, since several processes may be involved. The TSDC study has revealed a strong component of space-charge processes, although it is not possible to assure that space-charge processes are the only ones responsible for the polarization observed at high temperatures. We should not underestimate the uncertainty related to the nature of electrode-sample interface and the physical-chemical structure of the materials. A more detailed study should also take into account the effect of experimental conditions.

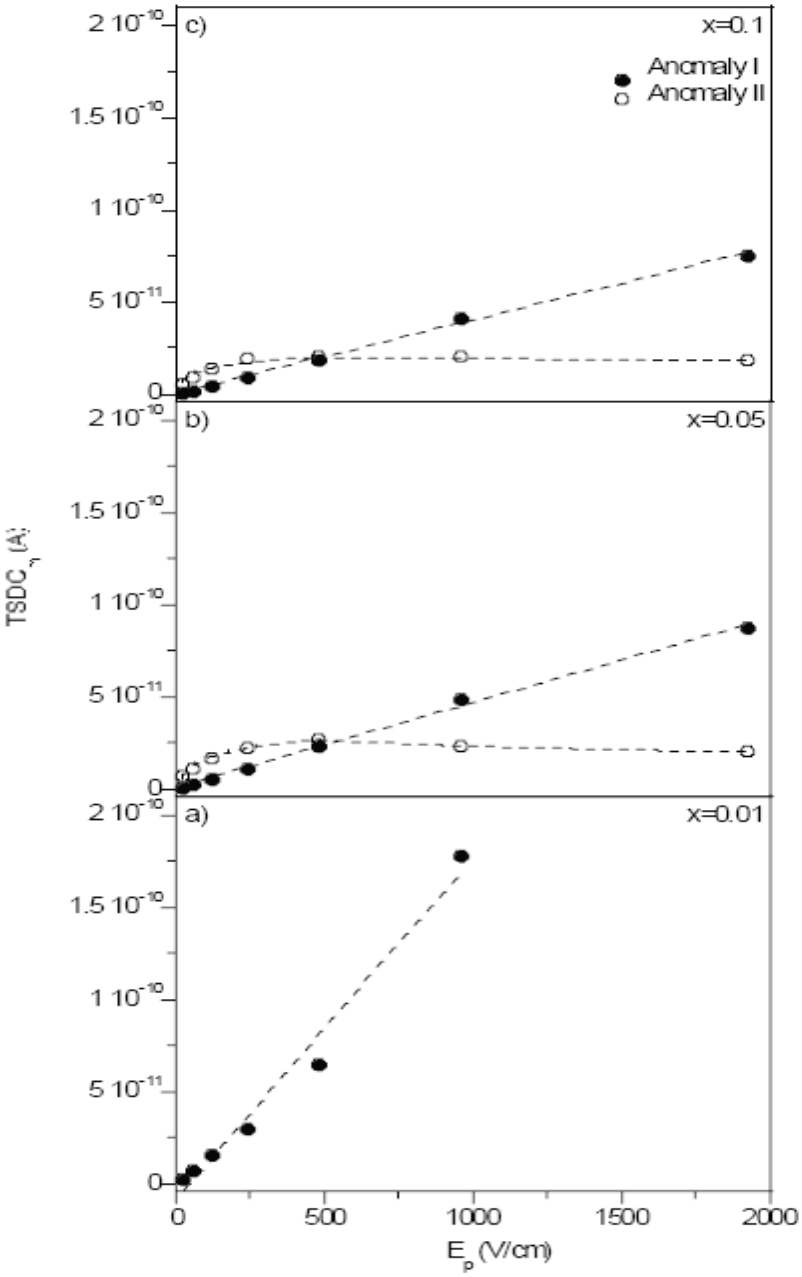

Figure 3-8 Field dependence of the maximum amplitude for a) x=0.01, b) x=0.05 and c) x=0.1 of anomaly I and II.

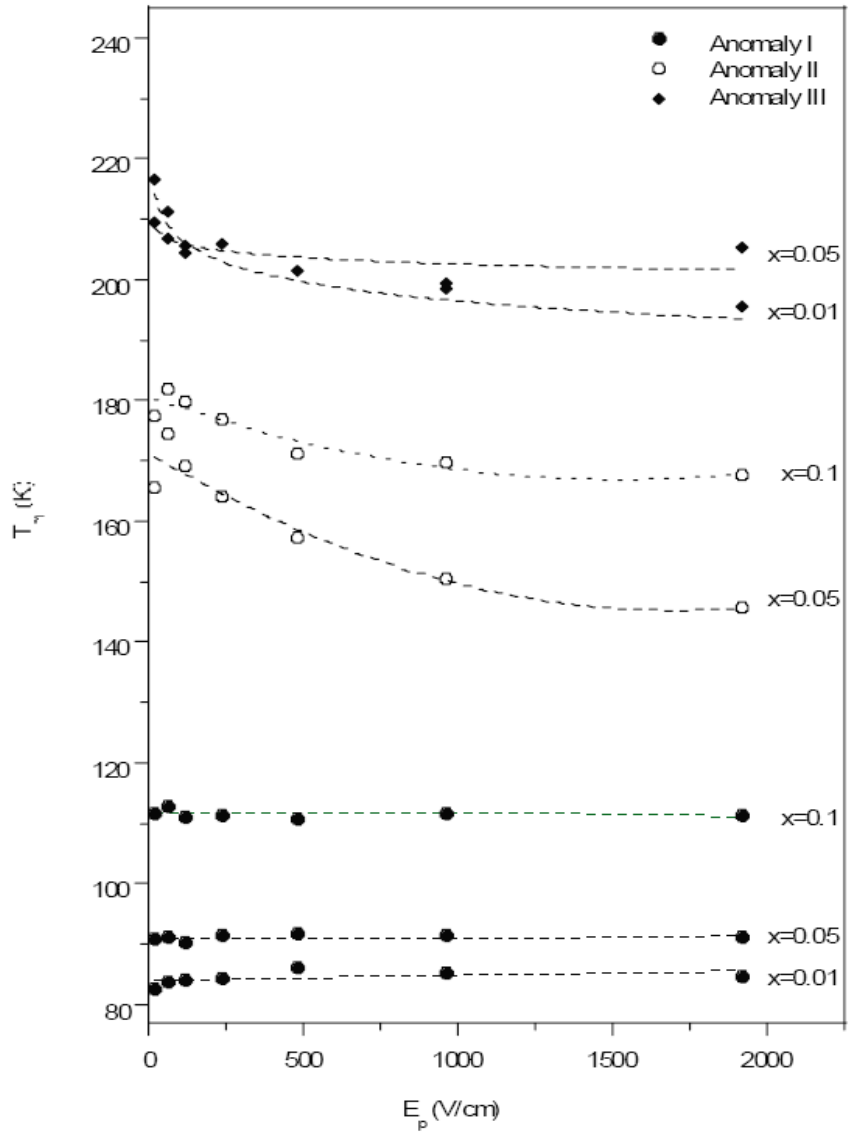

Figure 3-9 Field dependence of maximum amplitude temperature of different anomalies, for x=0.01, x=0.05 and x=0.1

Bucci and Fieschi model[36] was used to calculate the characteristic parameters of the dipolar relaxation process associated with anomaly I. This procedure enables us to obtain some important parameters, like relaxation time at infinite temperature and activation energy of the dipolar mechanism underlying this anomaly.

The results are summarized in Figure 3-10 and 3-11, where one can observe the activation energy (E_a) and the relaxation time at infinite temperatures (τ_o) for anomaly I as a function of the polarizing electric field E_p.

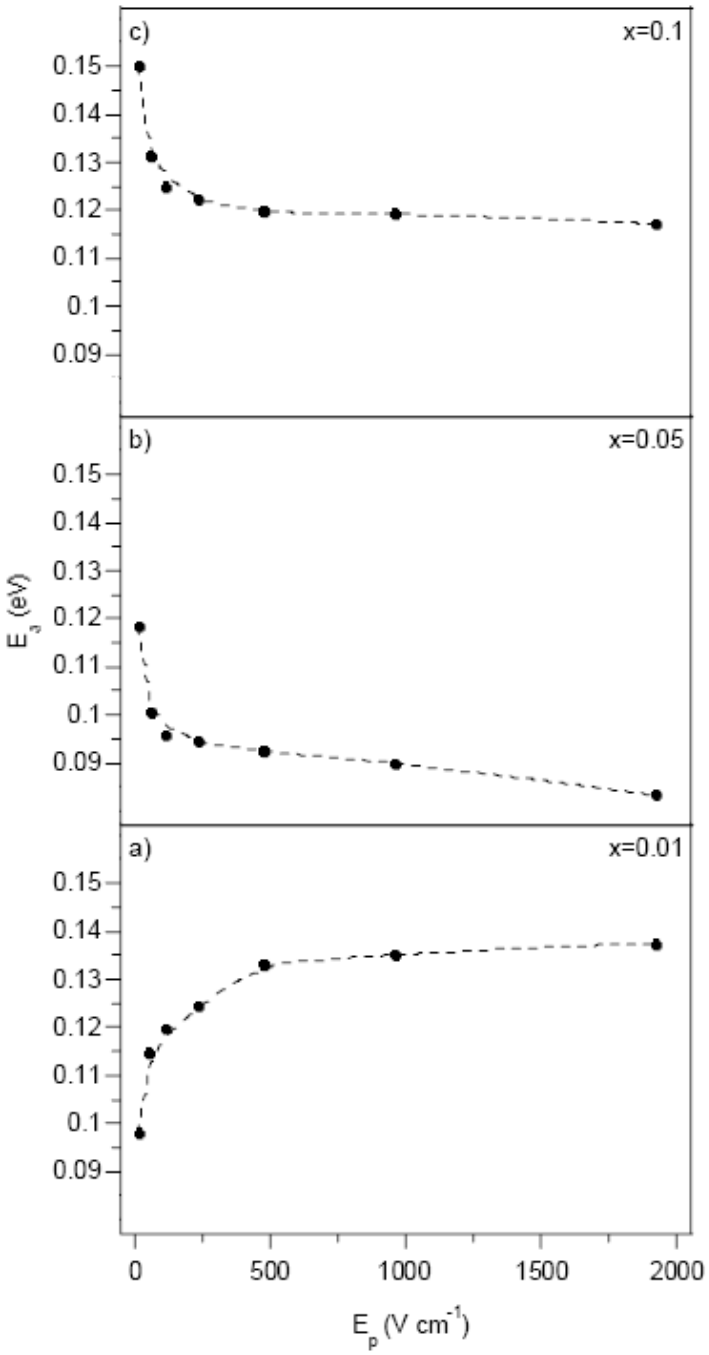

Figure 3-10 Field-dependence of the activation energy (E_a) of anomaly I and for a) x=0.01, b)0.05 and c)0.1.

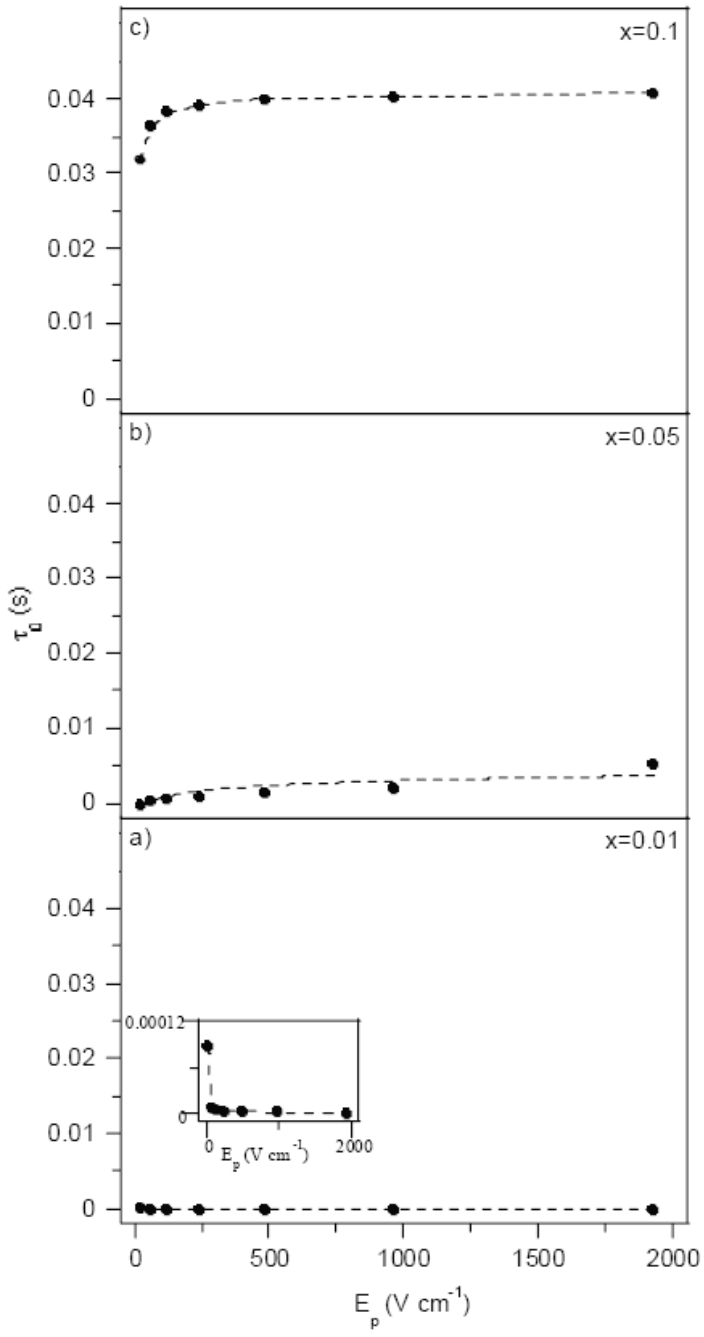

Figure 3-11 Field dependence of the relaxation time at infinite temperature (τ_o) of anomaly I and for for a) x=0.01, b) 0.05 and c) 0.1.

The field behaviour of activation energy at low fields E_p< 200 V/cm changes rather fast while for higher fields it becomes nearly constant. Despite the similarities referred to

above, $E_a(E_p)$ for the lowest concentration of Lanthanum is very different from the other two. It increases for lower fields and then nearly saturates at ~0.14 eV. Conversely, the other two anomalies are alike, though $E_a(E_p)$ is shifted to higher values as Lanthanum concentration increases. These results provide evidence for the existence of different types of relaxation mechanisms if one considers the activation energy behaviour. One expects, for lower Lanthanum concentration, random field dipolar reorientation to play a major role along with dipolar grain effects associated with structural freezing and frustration phenomena. Hence, τ_o shifts to higher values as Lanthanum concentration increases (Figure 3-11). Nevertheless, for the lowest concentration, τ_o is several orders of magnitude lesser.

By using equation 3-2 and high-field values of the relaxation parameters for anomaly I, we have estimated the average value of the dipole density (N_d), where typical values for the electric moment (2×10^{-29} cm) and *s* (1/3) were assumed. An average dipole density of ~1×10^{22} dipoles/cm^3 was obtained.

From a practical application standpoint, like electrets, a large relaxation time at room temperature would be needed. Relaxation time τ at room temperature was estimated, using the Arrhenius law[33]: $\tau(T) = \tau_o e^{\frac{E_a}{kT}}$, and the high field values of E_a and τ_o. The calculated value of relaxation time at room temperature is ~ 300 s. This value of τ is clearly too low, which likely excludes the possibility of using La-doped $SrTiO_3$ ceramics as electret devices, at room temperature.

3.4 TSC of $Sr_{1-1.5x}Y_xTiO_3$ ceramics

This section concerns the study of TSC behaviour as a function of temperature and applied polarising field in Y-doped ceramics, in order to search for polar processes, and then attempt to identify the nature of the mechanisms involved.

Figure 3-12 shows the temperature dependence of TSC for x=0.01. Thermal cycling was carried out under a polarising electrical field of 1316 V/cm.

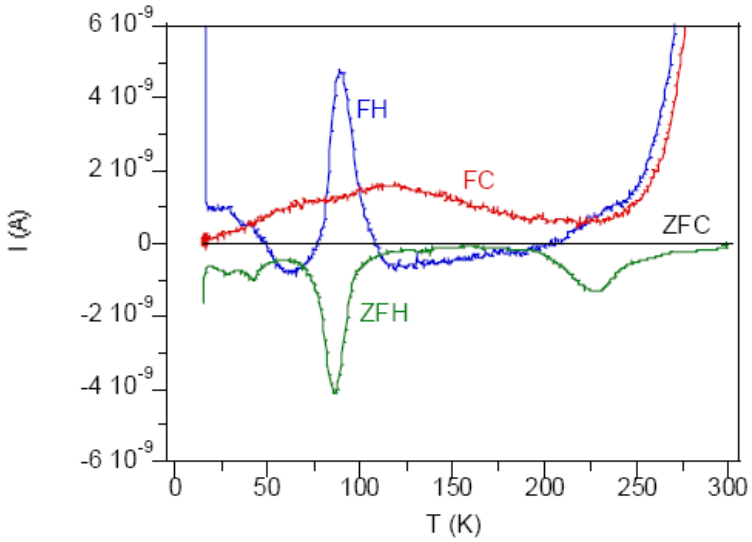

Figure 3-12 Thermal cycles, ZFC, FH, FC and ZFH for $Sr_{1-1.5x}Y_xTiO_3$ ceramics, x=0.01 under an applied field1316 V/cm.

As in La-doped $SrTiO_3$, no ZFC current is observed, thereby providing evidence of the absence of a ferroelectric state in this system as it have been reported[23]. The polarized currents (FH and FC currents) give us a clear indication of strong non-ergodic behaviour in doped Y systems.

In order to study TSD currents of $Sr_{1-1.5x}Y_xTiO_3$ (x=0.005 and 0.1), different polarized fields were applied to the ceramics. The results presented in Figure 3-13 are clearly indicative of different types of anomalies: anomalies I and II occurring in the temperature range 18-40 K and another six current peaks observed at T_{mIII}~70 K, T_{mIV}~85 K, T_{mV}~134 K, T_{mVI}~185 K, T_{mVII}~250 K and T_{mVIII}~286 K.

Figure 3-13 indicates that Yttrium doping drastically changes the intensity of all current anomalies, whilst no visible change is observed in their original position.

Figure 3-13 acknowledges the fact that the amplitude of both anomalies IV and VII becomes upon increasing the applied field though up to a certain point at which time then becomes constant. In addition, the temperature of its maximum is field independent.

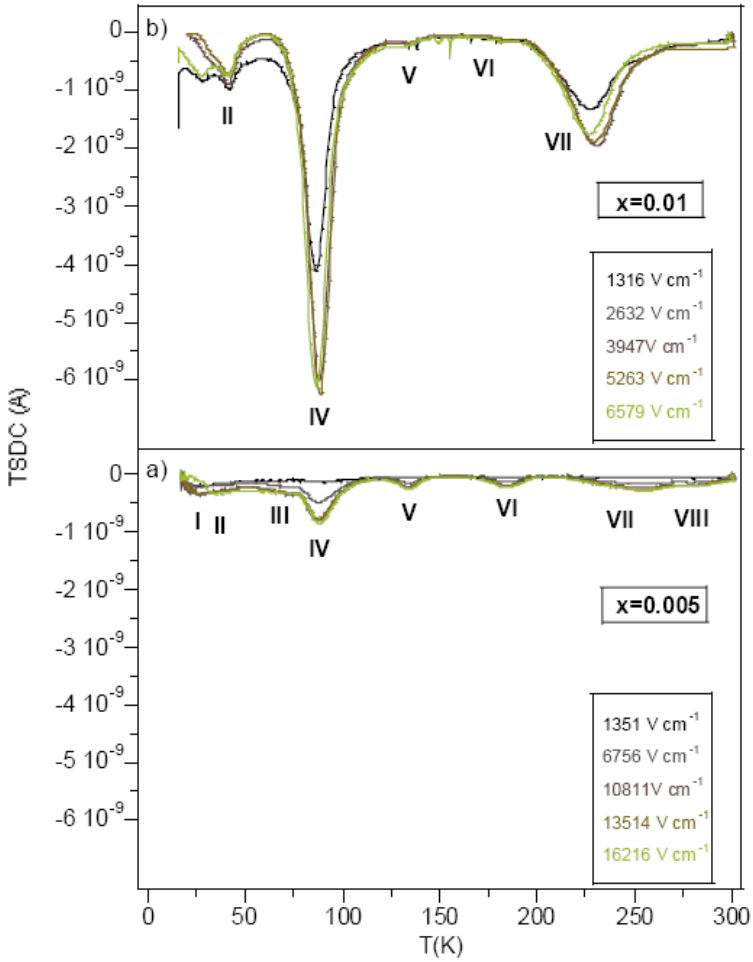

Figure 3-13 TSDC of $Sr_{1-1.5x}Y_xTiO_3$ ceramics, x=0.005 a) and x=0.01 b).

In order to characterize the nature of both IV and VII current peaks, the maximum amplitude of each peak and the corresponding temperature have been determined as a function of the polarizing field. Their field behaviour is displayed in Figure 3-14. In the present work we will focus on anomaly IV. Equation 3-6 was then fitted to the experimental data relative to this anomaly. Though the TSDC intensity of the anomaly does not show for the range of applied field used a linear behavior, the good quality of the fittings, its position invariance, as well as its location in the low temperature range provides clearly their dipolar nature.

The results are summarized in Figure 3-15, where we can observe activation energy (E_a) and relaxation time at infinite temperatures (τ_0) for both compositions as a function of the polarizing electric field E_p.

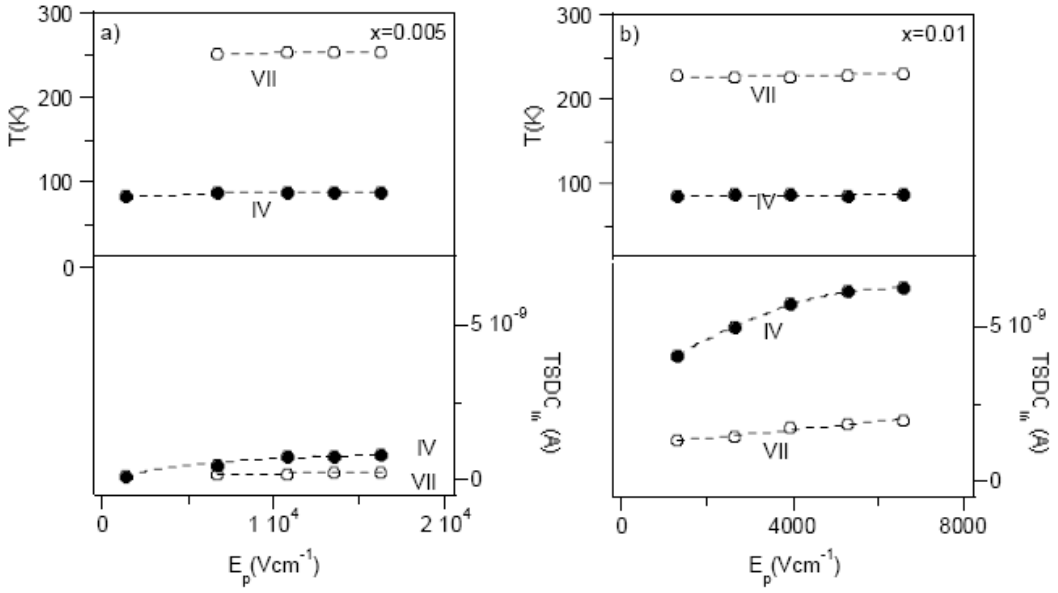

Figure 3-14 Maximum amplitude and corresponding tempertaure of current anomalies as a function of applied field, for x=0.005 a) and x=0.01 b).

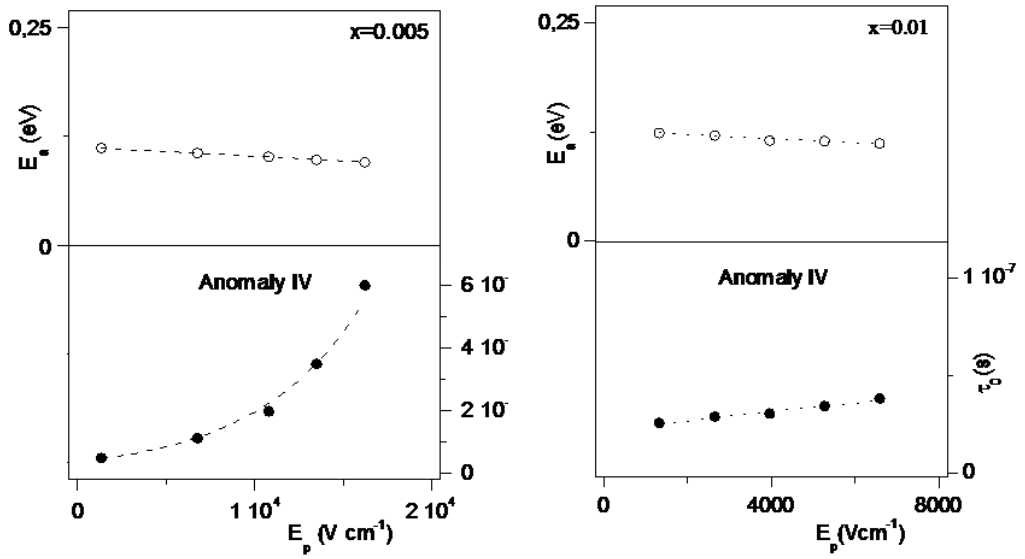

Figure 3-15 Activation energy and relaxation time for both anomalies IV a) and VII b) obtained in x=0.01 as a function of E_p.

For the ceramic with higher Yttrium concentration, E_a is ~10 % higher and τ_0 is approximately of the same magnitude than the ones observed for the lower concentration ceramic, with regard to the same range of electric field magnitude.

Though the relaxation parameters do not change significantly with Yttrium concentration, conversely the intensity of TSD currents drastically increase with increasing Yttrium content.

3.5 TSC of $Sr_{1-x}Mn_xTiO_3$ and $SrTi_{1-x}Mn_xO_3$ ceramics

Up to this point, this work has focused on the influence of A-site substitution by trivalent La^{3+} and Y^{3+} ions on TSD currents. In order to get better knowledge of the effect of doping $SrTiO_3$ ceramics, this section covers the study of thermal cycles and TSDC in $Sr_{1-x}Mn_xTiO_3$ ceramics, where isovalent substitution of Sr^{2+} by Mn^{2+} ions at the A-lattice site occurs. The study of Mn^{2+} B-site substitution is also included for comparison.

3.5.1 A-site substitution

Thermal cycles in $Sr_{1-x}Mn_xTiO_3$ ceramics, reveal features quite similar to La- and Y-doped $SrTiO_3$ (Figure 3-16): (i) Current thermal dependence is comparable for all compositions, (ii) no ferroelectric state is disclosed and, (iii) the poling procedure is an important aspect in determining the electrical behaviour of the system. Thus Manganese doping at the A-lattice site also leads to remarkable non-ergodic behaviour in $SrTiO_3$ ceramics.

As referred to above, the TSDC technique is a very helpful in characterizing the relaxation mechanisms that may arise in dielectrics. Figure 3-17 shows the temperature dependence of TSDC and corresponding polarisation P(T) in x=0.01, 0.02 and 0.05 at different fixed magnitudes of E_p. From Figure 3-17, one clearly sees a large anomaly located at ~ 25 K and others emergent at higher temperatures, though much smaller in intensity. In the ensuing section, we will focus our attention on the behaviour of the large low temperature anomaly.

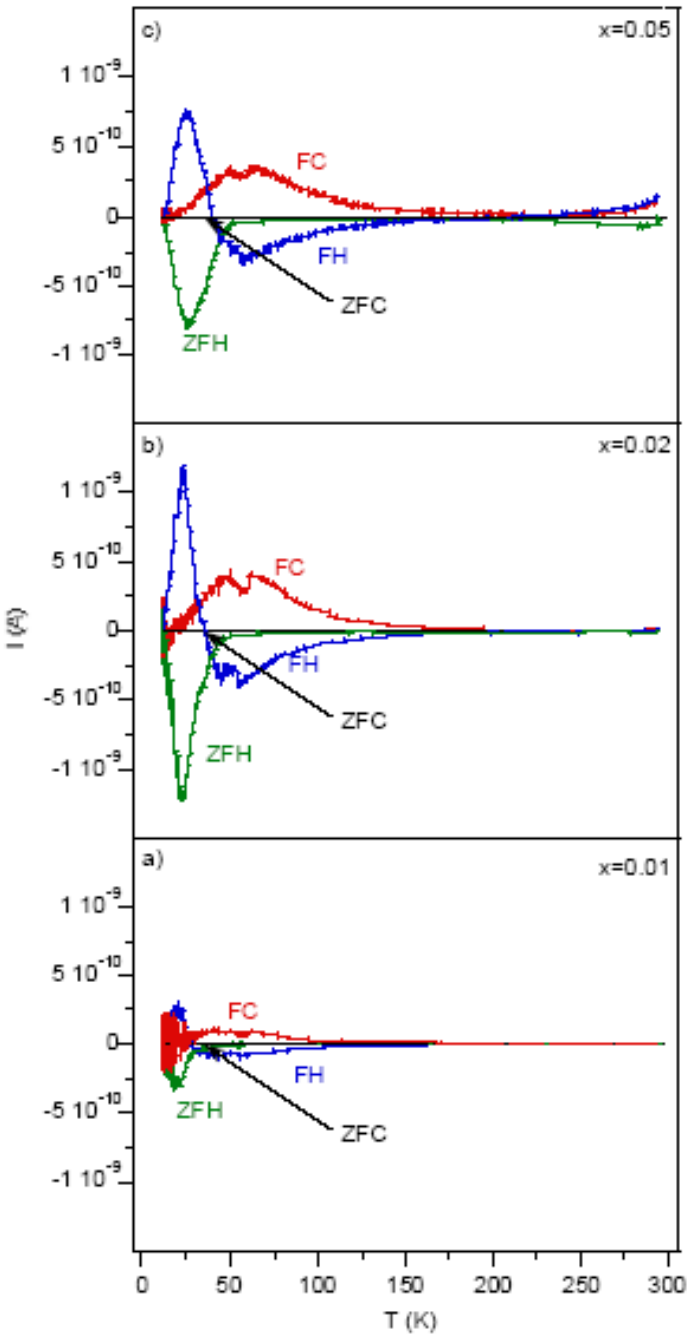

Figure 3-16 Temperature dependence of ZFC-FH-FC-ZFH electric currents under a field of 2222 V/cm, for a) x=0.01, b) x=0.02 and c) x=0.05

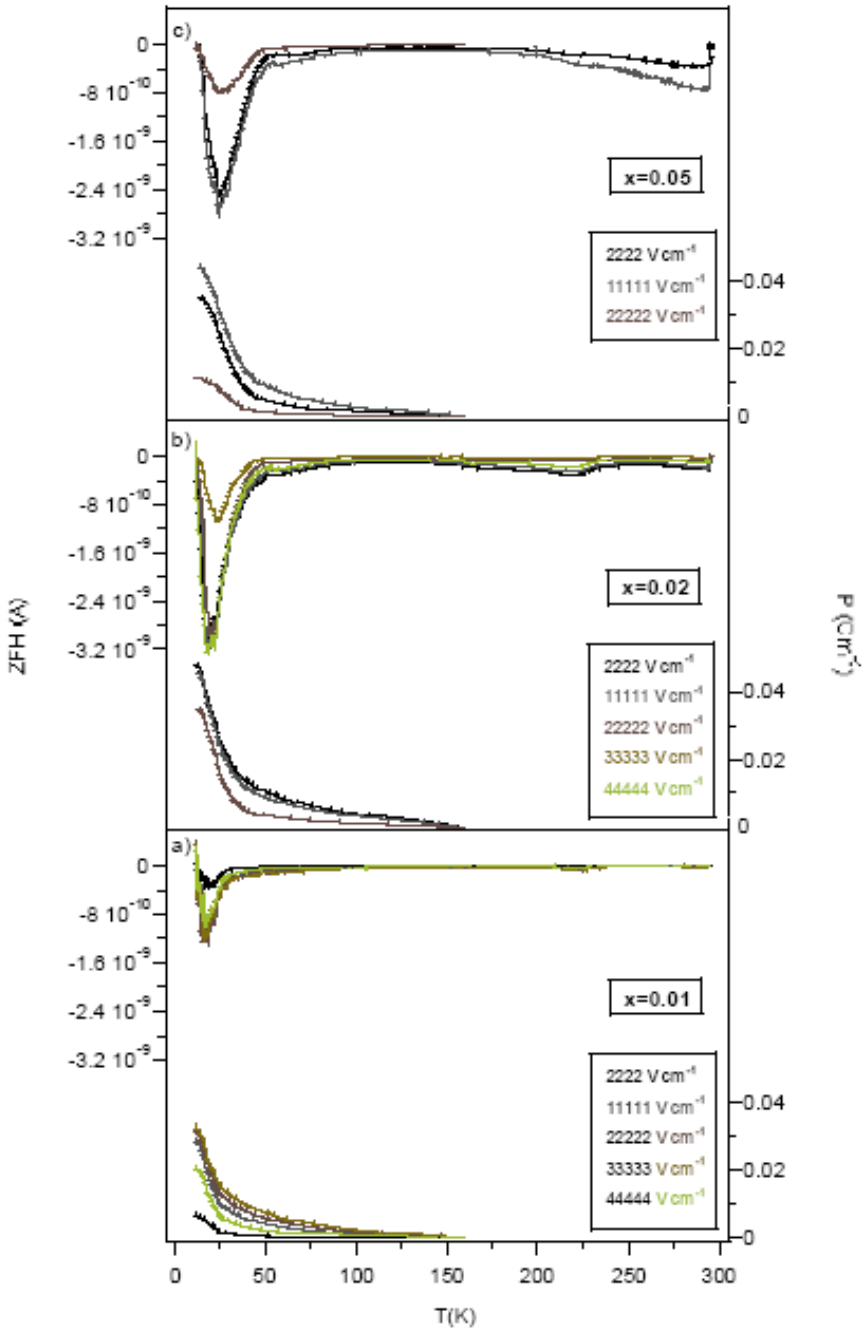

Figure 3-17 TSDC and polarization as a function of the temperature at different fixed polarizing field E_p for a)x=0.01, b) x=0.02 and c) x=0.05 Sr^{2+}-site substitution.

This anomaly is clearly dependent on Manganese concentration in as far as its position and intensity is concerned. However, the intensity of the low temperature anomaly also reaches a limit value for all concentrations by applying an E_p> 2500 V/cm. This fact reveals that Manganese doping at A-site allows for an easier reorientation of the dipole system, which is in good agreement with previous results reporting the existence of low temperatures hysteresis loops and a decrease in the tolerance factor along with A-site Manganese substitution. Unlike heterovalent La^{3+} and Y^{3+}, isovalent Mn^{2+} doping does not exhibit any visible anomaly at ~ 80 K. This striking difference will be discussed in later sections.

Rather high values of the polarization can be observed, but only below ~ 25 K. This characteristic makes the usage of these systems in practical applications close to the room temperature difficult.

The model of Bucci *et al.*[36] was used to calculate the characteristic parameters of the dipolar relaxation processes associated with the low temperature anomaly. After attempting the fitting of experimental data to just one dipolar relaxation process, it turned out that this procedure would result in the unsatisfactory fitting quality. So two dipolar relaxation processes have been used instead.

The results are summarized in Figure 3-18 and 3-19 where we can observe the activation energy (E_a) and the relaxation time at infinite temperatures (τ_o) as a function of the polarizing electric field E_p of both processes.

From both figures and Table 3-1, one may observed that whilst $E_a(E_p)$ decreases, $\tau_o(E_p)$ increases when increasing field. The decrease of E_a is in good agreement with the fact that this system reaches polar saturation for relatively low values of the applied electric field. In addition, the composition with x=0.05 seems to return to the values for x=0.01, instead of following the behaviour suggested by the one observed for x=0.02.

An explanation for this unexpected feature could be based on the tendency of this system to form second phases for relatively low values of Manganese concentration[17].

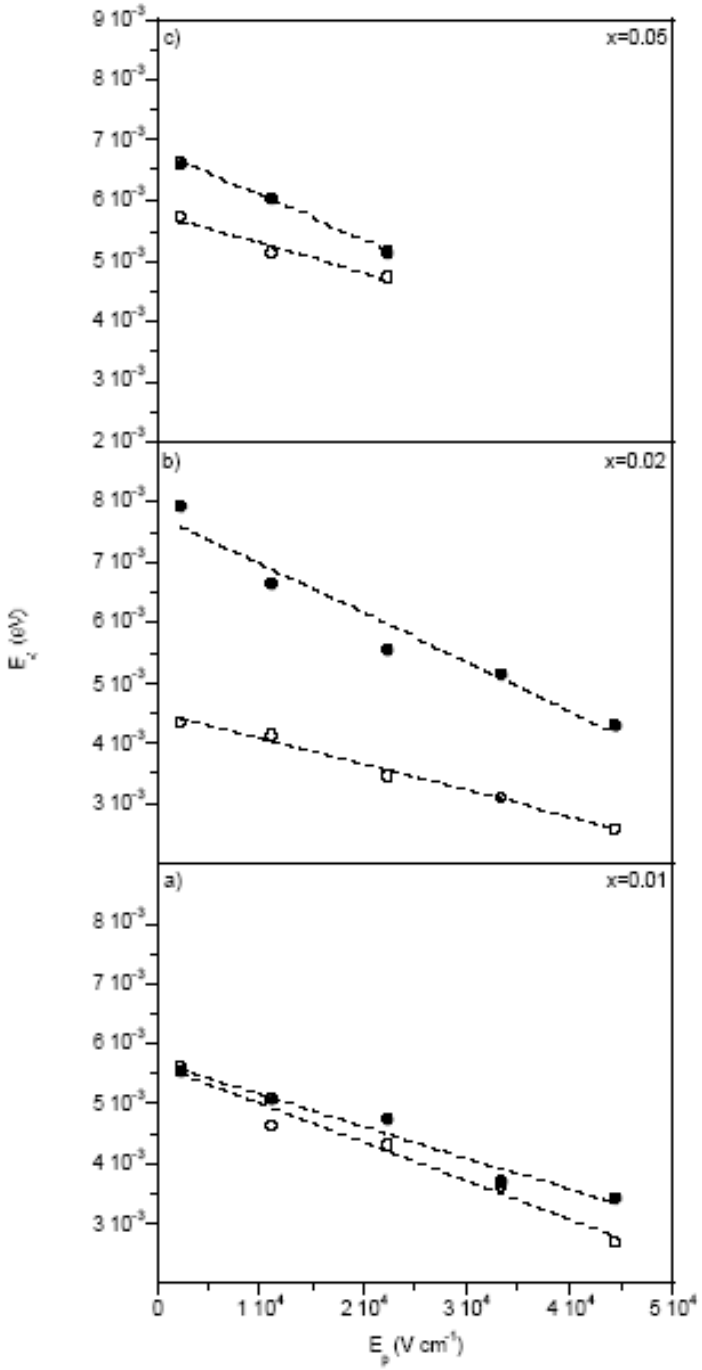

Figure 3-18 Field dependence of activation energies (E_a) for a) x=0.01, b) x=0.02 and c) x=0.05 relative to both dipolar relaxation processes.

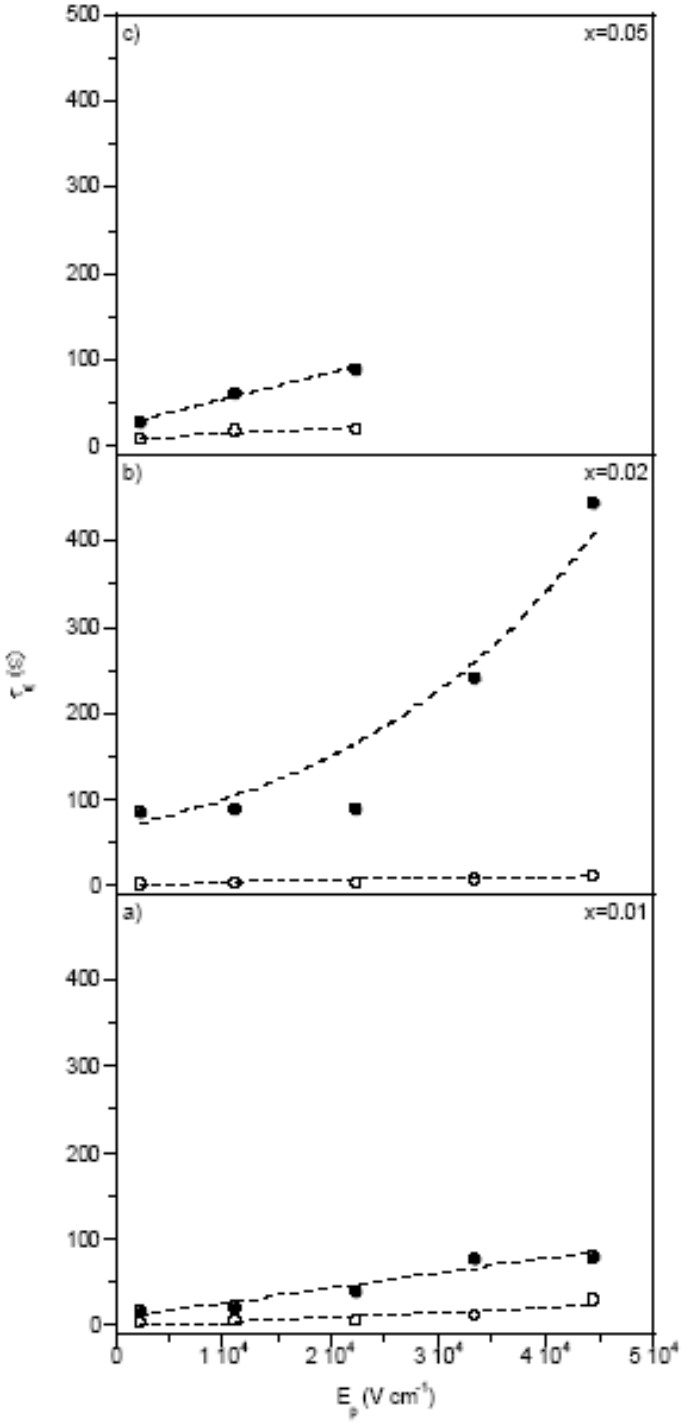

Figure 3-19 Field dependence of the relaxation times at infinite temperature (τ_o) for a) x=0.01, b) x=0.02 and c) x= 0.05 relative to both dipolar relaxation processes.

x	Ea (eV)	τ_o (s)
0.01	0.0055	15.5
0.02	0.0079	85.2
0.05	0.0066	27.4

Table 3-1 Relaxation parameters at 2222 V/cm for different Manganese concentrations.

For the $Sr_{1-x}Mn_xTiO_3$ system, the highest relaxation time at room temperature achieved was ~534 s, for ceramic with 2% of Manganese, when an electric field of 4444V/cm was applied. As in La- doped $SrTiO_3$ ceramics, this value is still quite low for practical applications at room temperature.

3.5.2 B-site substitution

TSDC and corresponding polarization P(T) in $SrTi_{1-x}Mn_yO_3$ (y=0.01 and 0.05) doped $SrTiO_3$ ceramics are displayed in Figure 3-20. Their temperature behaviour is very different for the one exhibited by an A-site manganese doped $SrTiO_3$ system. Though, some anomalies occur at similar temperatures, their intensities change with the applied field in very different ways. This is in line with the previously observed structural and microstructural data that have shown finer grains and lower tolerance factor comparatively with $Sr_{1-x}Mn_xTiO_3$ ceramics.

According to the above mentioned theory, the large anomaly is apparently associated with a depolarizable relaxation process. The decrease of its intensity with increasing Manganese concentration is probably due to the polarizability of the Manganese ion, which is smaller than that of the substituted Ti^{4+} ion located at the B-lattice site.

The broad complex anomaly observed for y=0.05 at 105 K, which is much larger than the one for y=0.01, is most certainly associated with space-charge polar processes, inducible through complex defect compensation[20].

The broad complex anomaly observed for y=0.05 above 105 K, which is much larger than the one for y=0.01 is certainly due to space-charge polar processes, apparently associated with the complex defect configuration existent in these systems.

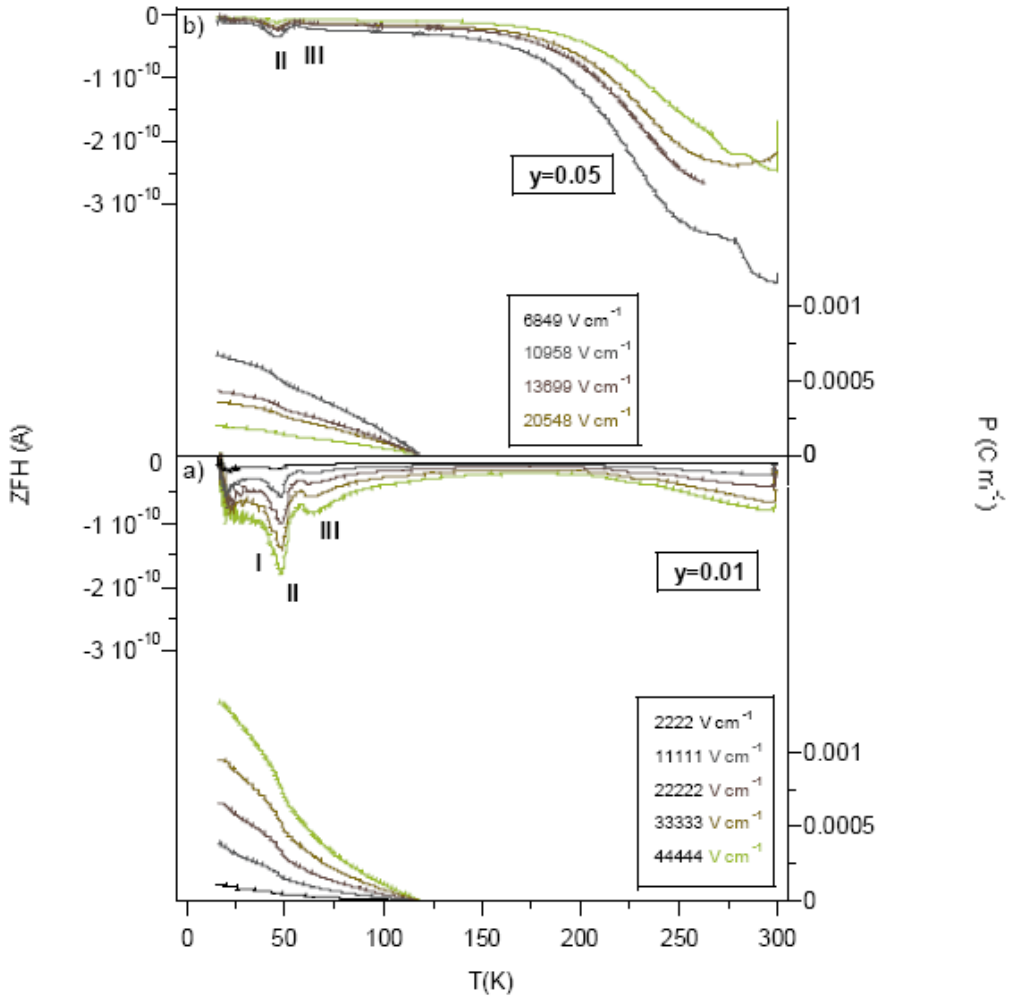

Figure 3-20 TSDC and polarization as a function of the temperature at different fixed polarizing field E_p for a) y=0.01, b) y=0.05 Ti-site substitution.

3.6 Discussion and Conclusion

TSC measurements were carried out for different selections of dopant ions, the characteristics of which are summarized in Table 3-2 along with those for Sr^{2+} and Ti^{4+}. The whole set of thermal cycle measurements corresponding to Lanthanum, Yttrium, and Manganese doping at the A-site evidences that no ferroelectric state is stabilized at low temperatures which sustain previous dielectric spectra observations[11,13,19]. This

means that polar states revealed by the appearance of slim P-E cycles[12] should be attributed to other kinds of states apparent in Mn^{2+} doping.

Ions	A-lattice site		B-lattice site	
	Oxidation state	Radius (A)	Oxidation state	Radius (A)
Manganese	+2	1.27	+4	0.53
Yttrium	+3	1.25	-	-
Lanthanum	+3	1.37	-	-
Strontium	+2	1.44	-	-
Titanium	-	-	+4	0.61

Table 3-2 Oxidant state and radius of Sr^{2+} and Ti^{4+} ions and dopants.

Results previously reported[12] in these systems are indicative of a polar relaxation state at low temperatures, associated with random distributed dipoles stemming from off-centre shifts of Mn^{+2} ion at A-lattice site.

The results obtained from TSDC measurements performed in La-, Y-, and Mn-doped $SrTiO_3$ ceramics provide evidence for the existence of a complex mechanisms contributing to their polar behaviour. This set includes different dipolar-type relaxation processes mainly located at lower temperatures, as well as processes associated with space charge displacements and eventually other ones due to formation of charge layers at the interfaces, expected to occur at higher temperatures. The next part of this section will be exclusively focused on polar processes associated with dipolar relaxation mechanisms.

TSDC results obtained by doping $SrTiO_3$ ceramics at A- and B-sites revealed that the corresponding dipolar relaxation mechanisms have different characteristics. In fact, dipoles induced by off-centre relaxation are strongly dependent on the symmetry and chemical coordination of the lattice site where the dopant ion is introduced, as well as on the number of possible energy minima available. Indeed the study of TSD currents carried out in doped $SrTiO_3$ ceramics, where the dopant ion is introduced at the A-site,

demonstrated the existence of different relaxation processes depending on the ion characteristics of the dopant. Isovalent (Mn^{2+}) and heterovalent (La^{3+}, Y^{3+}) substitution leads to different kinds of relaxation mechanisms, clearly evidenced by the different activation energies involved (see Table 3-3).

Dopant	E_a (eV)
La^{3+}	0.14
Y^{3+}	0.19
Mn^{2+}	0.006

Table 3-3 Activation energy for La^{3+}, Y^{3+} and Mn^{2+} (x=0.01) for Ep~2000 V/cm.

The main difference is the existence of Sr^{2+} vacancies in the case of La^{3+} and Y^{3+} doping, and that are required to ensure charge neutrality. Thus, the largest anomaly located ~90 K and with activation energy ~0.13 eV obtained for heterovalent substitution should be linked to dipoles associated with both off-centre ions and Sr^{2+} vacancies. However, La^{3+} ions have a more relevant role than those of Y^{3+}. In the former case, the anomaly shifts to higher temperatures with increasing Lanthanum concentration, whilst in the latter, its position does not visibly change. The explanation for this different behaviour is not clear, though the smaller ionic radius of the Y^{3+} ion relative to that of La^{3+} ion might play distinct role here.

Dielectric relaxation data for Lanthanum doping, reported previously, also provide evidence for the existence of such kinds of polar relaxation mechanisms with similar values of the activation energy, as shown in Table 3-4.

The corresponding anomaly in TSDC obtained from isovalent Manganese doping has a much smaller activation energy ranging from 0.003 to 0.007 eV, thus located at lower temperatures (~25 K), when compared to that obtained from heterovalent doping. Assuming that for Manganese doping there are no Sr^{2+} vacancies, randomly distributed dipoles must stem mainly from off-center Mn^{2+} ions.

Recently, measurements performed in Ca^{2+} doped $SrTiO_3$ ceramics also revealed an anomaly in TSDC with similar temperature position and activation energy, which

confirms that in the case of isovalent doping, the most important source of random dipoles is the off-centre position of the doping ion.

	E_a (eV)	
	TSDC	**Dielectric spectra**
La^{3+} (x=0.1)	> 0.12	0.31

Table 3-1 Activation energy obtained by TSDC and Dielectric spectra measurements for La-doped $SrTiO_3$.

Though different in time scale, TSDC and dielectric relaxation techniques can thus be used to obtain complementary information, useful in gaining a more comprehensive understanding of polar mechanisms in doped $SrTiO_3$ ceramics.

4 Conclusions and Further Work

4.1 Conclusions

Although $SrTiO_3$ related materials have been widely utilized for practical applications, their dynamics and polar relaxation behaviour are still not very well understood. This understanding will be crucial to expand the existing applications to the nano-microelectronics applications, in which size effects control the material response.

In this work, La- and Y-doped $SrTiO_3$ ceramics were studied through Raman and TSC techniques. The experimental data were analysed by adequate theoretical models, and discussed towards identifying the most relevant lattice and polar mechanisms involved.

Raman spectroscopy data of La- and Y-doped $SrTiO_3$ ceramics have revealed interesting new features, when compared with results previously reported for the undoped one. Despite some small differences observed in intensity, width and position of Raman active modes, and the shift of the whole spectra to higher temperatures, there is a good agreement between temperature behaviour of modes both for doped and undoped systems.

In order to obtain the shift of the paraelectric-antiferrodistortive phase transition temperature T_a, the thermal dependence of the E_g and B_{1g}, as well as the softening A_{1g} Raman modes were thoroughly studied. A shift of T_a towards higher temperatures has been observed for both systems, which is directly dependent on ionic radius of the dopant, and its concentration. The shift of T_a can be explained by the decrease of tolerance factor, whose value is partially dependent on the dopant radius, though not alone. The observed increase of T_a by Raman agrees well with the previous observation of the modification of T_a by in situ TEM.

It has been previously reported that at low temperatures quantum fluctuations can be depressed by doping $SrTiO_3$ lattice with some specific impurities. In fact, some dopants may lead to a ferroelectric at low temperatures. However, for La- and Y-doped $SrTiO_3$ ceramics, such a state does not occur as Raman active TO_1 polar mode does not completely softens. This observation has been also confirmed by TSC measurements, since no Zero-Field-Cooling current was detected. In addition these results are in agreement with the previously reported dielectric characterization of these systems.

Though Mn-doped $SrTiO_3$ ceramics present slim P-E hysteresis loops at low temperatures, a polar relaxor state is stabilized instead of a ferroelectric one.

Thermal cycles obtained in La-, Y-, and Mn-doped ceramics have revealed that these systems are non-ergodic and do not exhibit a ferroelectric state at low temperatures, in good agreement with Raman results referred to above and the previously reported dielectric studies. A semiconductor behaviour in Lanthanum doped system could also be disclosed.

TSDC studies performed in La-, Y-, and Mn-doped systems have revealed the existence of dipolar-type relaxation processes located mostly at lower temperatures, as well as other ones associated with space charge displacements, which occur mainly at higher temperatures, in a good agreement with the dielectric response of each of these systems.

It was also proved that the dipolar relaxation mechanisms have different characteristics, depending on A- or B- lattice site substitution of $SrTiO_3$.

TSD currents measurements carried out in doped ceramics, where the dopant ion is introduced at the A-site of the lattice showed that relaxations processes are strongly dependent on whether isovalent or heterovalent substitution takes place. In the later case, Sr^{2+} vacancies play an important role in the formation of random dipoles associated with the corresponding relaxation process, whilst for the former one the contribuition for dipoles' formation comes alone from the off-centre position of the dopant ion.

The obtained results agree well with the dielectric relaxation data for Lanthanum and Yttrium doping previously reported and confirm that polar relaxation mechanisms referred to above do exist with similar values of the activation energy.

4.2 Further work

Future work should address the following points:

- A study of doped $SrTiO_3$ ceramics with different grain size should be performed to describe the role of grain in lattice dynamics and relaxation mechanisms.
- With the objective of differentiating the mechanisms involved in polar states at higher temperatures, a different experimental set-up should be employed. An insulator layer should be included between the sample and electrode to avoid

migration of free charges at the interface. Thus, a deeper analysis could be carried out on space-charge relaxation mechanisms.

- A similar study should be undertaken for the same doped systems but in single crystals. This would enable the influence of granular nature in lattice dynamics and relaxation processes to be assessed more efficiently.
- In ceramics, grain boundaries can play an important role in their properties. Hence, to clarify the actual sources for the formation of random distributed dipoles, atomic force microscopy based techniques at low temperatures should be performed both within the grains and at different positions located at the grain boundaries.

REFERENCES

[1] http://www.emg.tu-bs.de/bilder/forschung/material/srtio3.jpg

[2] Müller, K. A., Burkard, H., Phys. Rev. B **19**, p. 3593 (1979)

[3] Hemberger, J., Lunkenheimer, P., Viana, R., Böhmer, R., Loidl, A., Phys. Rev. B **52**, p. 13159 (1995)

[4] Worlock, J. M., Fleury, P. A., Phys. Rev. Lett. **19**, p. 1176 (1967)

[5] Hemberger, J., Nicklas, M., Viana, R., Lunkenheimer, P., Loidly A., Ohmer, R. B., J. Phys.: Condens. Matter **8**, p.4673 (1996)

[6] Müller, K. A., Berlinger, W., Tosatti, E., Zeitschrift für Physik B Condensed Matter, Vol. 84, Issue 2, p.277 (1991)

[7] Arzel L., Hehlen B., Tagantsev A. K.m Denoyer F., Liss K. D., Currat R., Courtens E., Ferroelectrics, Vol. 267, p.317 (2002)

[8] Scott, J. F., Ledbetter, H., Z. Phys. B **104**, p.635 (1997)

[9] Petzelt, J., Ostapchuk, T., Gregora, I., Rychetský, I., Hoffmann-Eifert, S., Pronin, A. V., Yuzyuk, Y., Gorshunov, B.P., Kamba, S., Bovtun, V., Pokorný Savinov, M., Porokhonskyy, V., Rafaja, D., Vanek, P., Almeida, A., Chaves, M. R., Volkov, A.A., Dressel, M., Waser, R., Phys. Rev. B **64**, p.184111-1 (2001)

[10] Petzelt, J., Ostapchuk, T., Gregora, I., Kuzel, P., Liu, J., Shen, Z., J. Phys.: Condens. Matter **19**, p.196222, (2007)

[11] Almeida, A., Chaves, M. R., Gregora. I., Muga, N. J., Vilarinho, P. M., Kholkin, A. L., Costa, A. M., Ferroelectrics **318**, p.147 (2005)

[12] Tkach, A., Vilarinho, P.M., Kholkin, A.L., Applied Physics Letters, **86**, p.172902 (2005)

[13] Zhi, Y., PhD Thesis, Universidade de Aveiro, Aveiro, Portugal (1997)

[14] Tkach, A., PhD Thesis, University of Aveiro, Aveiro, Portugal (2005)

[15] Tien, T. Y., Cross, L. E., Jap. Journal Applied Physics **6**, p.459 (1967)

[16] Tkach, **A.,** Vilarinho, **P.M.,** Reaney, I. M., Accepted in Microscopy and Microanalysis On Line Journal (2008)

[17] Tkach, A., Vilarinho, P.M., Kholkin, A., Acta Materialia **53**, p.5061 (2005)

[18] Tkach, A., Vilarinho, P.M., Kholkin, A., Ferroelectrics **304**, p.87 (2004)

[19] Iguchi, E., Lee, K.J., Journal of Material Science, Vol. 28, Issue 21, p.5809 (2003)

[20] Tkach, **A.,** Vilarinho, **P.M.,** Kholkin, Reaney, I. M., Pokorny, J., Petzelt, J., Chemistry of Materials **19** (26), p.6471 (2007)

[21] Hui, S., Petric, A., J. Eur. Ceram. Soc. **22**, p.1673 (2002)

[22] Fu, Q.X., Mi, S.B., Wessel, E., Tietz, F., J. Eur. Ceram. Soc. **28**, p.811 (2008)

[23] Wang, R., Inaguma, Y., Itoh, M., Physica B, p.284 (2000)

[24] Burn, I, Neirman, S., J. Materials Science **17**, p. 3510 (1982)

[25] Müller, K. A., Phys. Rev. Lett. **2**, p.341 (1959)

[26] Lemanov, V.V., Smirnova, E.P., Ukhin, E. V., Phys. Solid State **46**, p.1323 (2004)

[27] Tkach, A., Vilarinho, P.M., Kholkin, A., Pashkin, A., Veljko, S., Petzelt, J., Phys. Rev. B **73**, p.104113 (2006)

[28] Raman Spectroscopy, D.A. Long, New York: McGraw-Hill, (1977)

[29] Tritt-Goc, J., Pislewski, N., Szczepanska, L., Goc, R., Solid State Communications **108**, p.189 (1998)

[30] Almeida, A., Sarmento, S., Ribeiro, J.L., Vieira, L. G., Chaves, M. R., Klöpperpieper, A., Ferroelectrics **295**, p.9 (2003)

[31] Yamanaka, A., Kataoka, M., Inaba, Y., Inoue, K., Hehlen, B., Courtens, E., Europhys. Lett. **50** (5), p.688 (2000)

[32] Vanderschueren, J.,Gasiot, J., Springer-Verlag, Berlin, Ed. Bräunlich, P., p.135 (1979)

[33] Theory of Dielectrics, H. Fröhlich, Oxford University Press, London,UK, 1958

[34] Turnhout, J.V., Elsevier Scientific Pub. Co., Amsterdam; New York (1975)

[35] Marina, O., Canfield, N., Stevenson, J., Solid State Ionics **149**, p.21 (2002)

[36] Bucci, C., Fieschi, R., Guidi, G., Phys. Rev. **48**, p.816 (1966)